© 2019. Published by The Company of Biologists Ltd | Development (2019) 146, dev172106. doi:10.1242/dev.172106

RESEARCH ARTICLE

A crucial role for Arf6 in the response of commissural axons to Slit

Mariko Kinoshita-Kawada[1,2,3], Hiroshi Hasegawa[4,*], Tsunaki Hongu[4,‡], Shigeru Yanagi[5], Yasunori Kanaho[4], Ichiro Masai[1], Takayasu Mishima[3], Xiaoping Chen[2], Yoshio Tsuboi[3], Yi Rao[6], Junichi Yuasa-Kawada[1,2,3,7,8,§] and Jane Y. Wu[2,§]

ABSTRACT

A switch in the response of commissural axons to the repellent Slit is crucial for ensuring that they cross the ventral midline only once. However, the underlying mechanisms remain to be elucidated. We have found that both endocytosis and recycling of Robo1 receptor are crucial for modulating Slit sensitivity in vertebrate commissural axons. Robo1 endocytosis and its recycling back to the cell surface maintained the stability of axonal Robo1 during Slit stimulation. We identified Arf6 guanosine triphosphatase and its activators, cytohesins, as previously unknown components in Slit-Robo1 signalling in vertebrate commissural neurons. Slit-Robo1 signalling activated Arf6. The *Arf6*-deficient mice exhibited marked defects in commissural axon midline crossing. Our data showed that a Robo1 endocytosis-triggered and Arf6-mediated positive-feedback strengthens the Slit response in commissural axons upon their midline crossing. Furthermore, the cytohesin-Arf6 pathways modulated this self-enhancement of the Slit response before and after midline crossing, resulting in a switch that reinforced robust regulation of axon midline crossing. Our study provides insights into endocytic trafficking-mediated mechanisms for spatiotemporally controlled axonal responses and uncovers new players in the midline switch in Slit responsiveness of commissural axons.

KEY WORDS: Slit-Robo, Axon guidance, Commissural neurons, Midline, Endocytic recycling, Arf6

INTRODUCTION

How developing axons grow towards their final targets is a fascinating question in neurobiology (Lewis et al., 2013). The roles of various neuronal guidance cues, which direct axon growth along particular routes, and their receptors in neural circuit formation have been clarified (Guan and Rao, 2003; Kolodkin and Tessier-Lavigne, 2011). Axons use intermediate guideposts to reach their targets. This strategy relies on an axon's ability to change its response to guidance cues at the right time and place.

Growing axons make a crucial decision at the ventral midline as to whether to cross it or not. Floor-plate (FP) cells at the midline act as guideposts by secreting attractive and repulsive guidance cues. Midline crossing by commissural axons is a powerful model for studying how axons switch on/off responses to guidance cues in a spatiotemporally regulated manner (Ducuing et al., 2018; Stoeckli, 2017). In vertebrates, extracellular cues derived from the FP and ventral neural tube promote commissural axon growth towards the midline. Upon reaching the midline, but not before this point, commissural axons lose their responsiveness to these cues, and acquire responsiveness to repellents, such as Slit and semaphorins (Brose et al., 1999; Kidd et al., 1999; Li et al., 1999; Zou et al., 2000), so that they properly cross the midline. After crossing the midline, axons maintain their responsiveness to midline repellents, ensuring that they exit the midline and never re-cross it. Although roundabout 3.1 (Robo3.1; in vertebrates) and commissureless (Comm; in *Drosophila*) suppress Slit responsiveness before axons reach the midline (Chen et al., 2008; Kidd et al., 1998; Sabatier et al., 2004), the mechanism by which axons increase Slit sensitivity upon midline crossing remains unclear. Comm prevents axonal transport and surface distribution of Robo by sorting Robo from the synthetic to the late-endosomal pathway (Keleman et al., 2002, 2005). A proline-rich and Gla domain gene, *Prrg4*, has been reported as a vertebrate Comm homolog (Justice et al., 2017). However, it is unknown whether similar endosomal trafficking modules are used in the vertebrate midline switch (O'Donnell et al., 2009).

Here, we have examined the mechanisms controlling Slit responsiveness of commissural axons. Our results showed that both Robo1 endocytosis and subsequent recycling are required for protecting surface-located Robo1 molecules at the time of Slit stimulation against degradation. Slit-Robo1 signalling activated ADP-ribosylation factor 6 (Arf6), in contrast to Robo4-mediated suppression of Arf6 (Jones et al., 2009). The Robo1 endocytic recycling-driven positive feedback, mediated by Arf6, enhanced axonal response to Slit upon midline crossing. Analyses of Arf6-knockout mice and cytohesin-knockdown neurons revealed that cytohesin Arf-GEFs (Arf-guanine nucleotide exchange factors) regulate Slit sensitivity before and after midline crossing. Thus, cytohesin-Arf6 pathways constitute an endocytic switch in Slit responsiveness. Our data provide insights into mechanisms underlying midline switching of commissural axon response to various guidance cues, including Slit and semaphorin proteins, and Sonic hedgehog (Shh).

RESULTS

Slit increases axonal Robo1 levels in commissural neurons

To study the mechanisms regulating the responsiveness of commissural neurons to Slit, we established a commissural neuron culture system that recapitulates the *in vivo* switch in Slit

[1]Developmental Neurobiology Unit, Okinawa Institute of Science and Technology Graduate University, Onna, Okinawa 904-0495, Japan. [2]Department of Neurology, Lurie Comprehensive Cancer Center, Northwestern University Feinberg School of Medicine, Chicago, IL 60611, USA. [3]Department of Neurology, Faculty of Medicine, Fukuoka University, Fukuoka 814-0180, Japan. [4]Department of Physiological Chemistry, Faculty of Medicine and Graduate School of Comprehensive Human Sciences, University of Tsukuba, Tsukuba, Ibaraki 305-8575, Japan. [5]Laboratory of Molecular Biochemistry, School of Life Sciences, Tokyo University of Pharmacy and Life Sciences, Hachioji, Tokyo 192-0392, Japan. [6]State Key Laboratory of Biomembrane and Membrane Biology, Peking-Tsinghua Center for Life Sciences, PKU-IDG/McGovern Institute for Brain Research, Peking University School of Life Sciences, Beijing 100871, China. [7]Center for Advanced Medical Innovation, Kyushu University, Fukuoka 812-8582, Japan. [8]Department of Clinical Chemistry and Laboratory Medicine, Kyushu University Graduate School of Medical Sciences, Fukuoka 812-8582, Japan.
*Present address: Department of Hygienic Sciences, Kobe Pharmaceutical University, Kobe 658-8558, Japan. ‡Present address: Heidelberg Institute for Stem Cell Technology and Experimental Medicine, German Cancer Research Center, Heidelberg 69120, Germany.

§Authors for correspondence (jkawada@cclm.med.kyushu-u.ac.jp; jane-wu@northwestern.edu)

J.Y.-K., 0000-0002-1382-3159; J.Y.W., 0000-0003-1794-1213

Received 22 September 2018; Accepted 14 January 2019

Development (2019) 146, dev172106. doi:10.1242/dev.172106

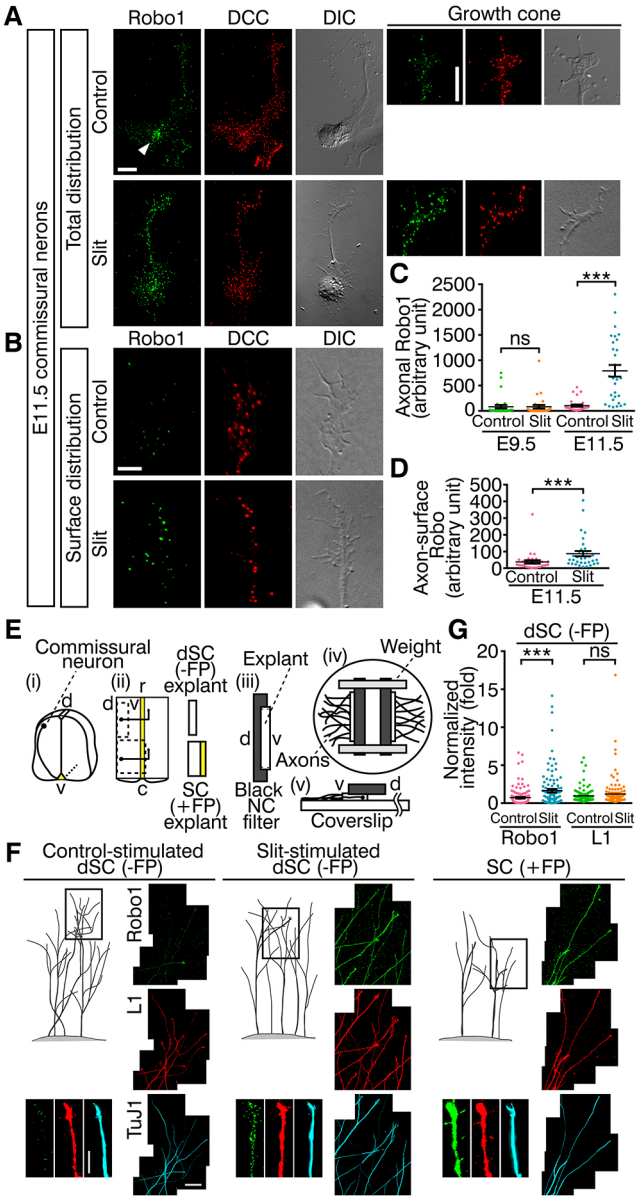

Fig. 1. Slit elevates axonal Robo1 levels in E11.5, but not E9.5, commissural neurons. (A-D) DCC$^+$ (red) commissural neurons from E11.5 mouse spinal cords were stimulated with 25 pM Slit for 10 min. Maximal-intensity projections of deconvoluted *z*-stacks of immunofluorescence and differential interference contrast (DIC) images are shown. Endogenous Robo1 (green) was detected with an antibody against the Robo1 extracellular domain. (A) Subcellular distribution of Robo1. Arrowhead indicates Robo1 localization to the perinuclear region of E11.5 commissural neurons, in the absence of Slit. (B) Robo1 expression on the distal axon surface. (C) Robo1 intensity in the distal-most 30 µm of axons (stained as in A). Data are mean±s.e.m. *n*=30 (neurons) (E9.5, results were from two independent experiments, 15 neurons/experiment; E11.5, three experiments, 10 neurons/experiment). E9.5, *P*=0.8111; E11.5, ***P<0.0001; two-tailed Mann–Whitney test. ns, not significant. (D) Distal axon-surface Robo1 levels (stained as in B; three experiments). *n*=41 and 42 (neurons) from left to right. ***P=0.0003. (E-G) Explant cultures of E11.5 spinal cords. (E) Schematics of spinal cord (SC) explant culture. (i) Commissural axon trajectory. d, dorsal; v, ventral. (ii) Open-book SC showing axon midline crossing. Dotted lines show cut placings to obtain dSC (–FP) or SC (+FP) explants (FP, in yellow). r, rostral; c, caudal. (iii) Explants mounted onto black nitrocellulose (NC) filters. (iv) Explants cultured on the coverslip. (v) Lateral view. (F) Representative results of dSC (–FP) explants stimulated with 25 pM Slit for 10 min and SC (+FP) explants. Schematic drawings of axon extension from explants, montage images (maximal-intensity projections corresponding to boxed areas) of axons triple stained for Robo1 (green), L1 (red) and β3-tubulin (TuJ1; cyan), and high-power images of distal axons are shown. (G) The effects of Slit on levels of Robo1 and L1 in axons extending from dSC (–FP) explants. Robo1 or L1 intensity in the distal axon was normalized to TuJ1 intensity and compared with control-stimulated neurons (four experiments). *n*=110, 114, 110 and 114 (distal axons). Robo1, ***P<0.0001; L1, *P*=0.8665. Scale bars: 10 µm in A; 5 µm in B; 50 µm in explant in F; 10 µm in axon in F.

responsiveness (Yuasa-Kawada et al., 2009a). Primary neuronal cultures were prepared from the cervical to lumbar levels of dorsal spinal cords of mouse embryos at embryonic day 9.5 (E9.5; when commissural axons have not reached the midline) and at E11.5-12.5 (when most axons have crossed the midline) (Altman and Bayer, 1984; Sabatier et al., 2004). The netrin receptor DCC (deleted in colorectal cancer) is broadly expressed in commissural neurons during midline-crossing stages in rats (corresponding to E9.5-11.5 in mice). We referred to dorsal spinal cord neurons whose axons were DCC positive as commissural, as in previously published studies (Keino-Masu et al., 1996; Okada et al., 2006; Yuasa-Kawada et al., 2009a) (Fig. 1A). Many DCC$^+$ neurons were also positive for Robo3; TAG-1, the first identified marker for commissural neurons (Dodd et al., 1988), localized to the cell body of commissural neurons, but less so to the axon, at E11.5 (Fig. S1A).

Commissural neurons from post-crossing stage embryos exhibited increased growth cone collapse responses following 30-min of Slit2 exposure, when compared with pre-crossing neurons (neurons were cultured for 2 days *in vitro* before stimulation) (Yuasa-Kawada et al., 2009a). Thus, in our culture system, commissural neurons maintained the memory of *in vivo* experience of midline crossing and acquiring Slit responsiveness.

To investigate whether Slit altered Robo distribution, dorsal spinal cord neurons were stimulated with Slit for 10 min, before growth cone collapse occurred. We immunostained endogenous Robo1 in fixed neurons (Fig. 1A) using an antibody against the Robo1 extracellular domain (for antibody specificity, see Long et al., 2004; Tamada et al., 2008; Yuasa-Kawada et al., 2009a; for Robo1 detection, see Fig. S1B). Because Robo1 is cleaved by metalloproteinases and γ-secretase (Seki et al., 2010), this anti-Robo1 antibody is postulated to detect full-length Robo1 and cleaved extracellular fragments. Robo1 expression was higher in E11.5 neurons than in E9.5 neurons (Fig. 1A and Fig. S1C–E). In E11.5 DCC$^+$ commissural neurons without Slit, Robo1 localized to the perinuclear region (Fig. 1A, arrowhead), with a lower level in the axons. After 10 min of stimulation with Slit, Robo1 levels in the distal axons increased significantly (Fig. 1A,C and Fig. S1G). This effect was specific, because axonal DCC levels were not markedly changed (Fig. S1D,F). In contrast, Slit did not affect axonal Robo1 levels in pre-crossing E9.5 commissural neurons (Fig. 1C and Fig. S1C). To examine whether Robo1was indeed redistributed to the axon surface upon Slit stimulation, we immunostained surface Robo1 in live neurons, without detergents, and found that Slit increased axon-surface Robo1 levels (Fig. 1B,D).

Furthermore, surface Robo1 levels in E12.5 dorsal spinal cord neurons were examined by extracellular biotinylation. Cell-surface proteins were biotinylated immediately after Slit stimulation, and collected using avidin-immobilized beads. Cell-surface Robo1 levels increased following a 10 min Slit stimulation (Fig. S1H). Next, we transiently transfected E11.5 dorsal spinal cord neurons with Robo1-GFP, and live-imaged Robo1-GFP dynamics. Slit induced the accumulation of Robo1-GFP into the growth cone (Fig. S1I).

To rule out a potential artefact associated with dissociated neurons, and to test for the effect of Slit in a more physiological

Development (2019) 146, dev172106. doi:10.1242/dev.172106

context, we prepared dorsal spinal cord explants lacking the FP and spinal cord explants containing the FP from E11.5 embryos (Fig. 1E). In both explant types, the extending axons were positive for L1, a post-crossing commissural axon marker (Dodd et al., 1988). In distal regions of commissural axons extending from dorsal spinal cord explants lacking the FP, Robo1 levels normalized to β3-tubulin (TuJ1) were significantly increased following Slit treatment (Fig. 1F,G). In FP-containing explants, Robo1 was distributed to post-crossing axons, without exogenous Slit treatment (Fig. 1F). These data indicated that Slit elevated Robo1 levels in post-crossing axons in dissociated commissural neurons and spinal cord explants.

Slit activates Robo1 endocytic recycling in commissural neurons

Co-immunostaining showed predominant overlaps of Robo1 with transferrin receptor (TfR) and Rab11 guanosine triphosphatase (GTPase), endocytic recycling compartment (ERC) markers, and partial overlaps with syntaxin 6, a trans-Golgi network (TGN) marker (Fig. 2A-C and Fig. S2A,B) (Bock et al., 1997; Stenmark, 2009). The ERC and TGN constitute major recycling stations to the cell surface (Maxfield and McGraw, 2004). By simultaneously examining intracellular trafficking of Robo1 and TfR from the cell-surface, we found that internalized Robo1 showed partial overlaps with transferrin (Tf), irrespective of Slit, suggesting that Robo1 was transported to the ERC (Fig. 2D and Fig. S2C). These observations led us to hypothesize that endocytosed and/or intracellularly stored Robo1 is mobilized to the axon surface via recycling pathways.

We therefore asked three questions: (1) are endocytosis and recycling involved in Slit-induced elevation of axonal Robo1 levels?; (2) does Robo1 protein surface-located at the time of Slit stimulation contribute to this elevation?; and (3) does Robo1 protein initially localized in intracellular pools contribute to this elevation? To address these questions, we analysed Robo1 trafficking during Slit stimulation in E11.5 commissural neurons using a series of live-cell antibody-feeding assays with anti-Robo (protein-A affinity-purified rabbit polyclonal antibody, composed of divalent IgG fractions; Fig. 2E and Fig. S2D). In Robo1-GFP-expressing neurons, after antibody labelling, internalized anti-Robo1 showed marked overlap with Robo1-GFP, indicating that most anti-Robo1 remained associated with the target Robo1 protein after internalization (Fig. S2E). In addition, a Slit-binding assay (Li et al., 1999), followed by blocking of cell-surface Robo1 and Slit, revealed that internalized Robo1 and Slit partially overlapped with each other (Fig. S2F), suggesting that, after endocytosis, at least some antibody labelled Robo1 proteins remained Slit-bound and signal competent.

Because Rab5 and Rab11 play crucial roles in endocytosis and recycling (Stenmark, 2009; Zerial and McBride, 2001), we used RNA interference (RNAi) against them to test the role of endocytic recycling (see Fig. 3B and Fig. S5A for specificity and efficiency of the RNAi). As shown in Fig. 2Ei and Fig. S2D, we labelled surface Robo1 in commissural neurons using anti-Robo1, before Slit or control stimulation. By immunostaining after stimulation, we monitored total pools of antibody-labelled Robo1, i.e. Robo1 molecules initially surface located. Initial levels (0 min) of antibody-labelled Robo1 in the distal axon were not significantly different between neurons transfected with small interfering RNAs (siRNAs) against Rab5 or Rab11 and control siRNA (siControl)-transfected neurons (Fig. 2F and Fig. S4A). In siControl-transfected commissural neurons, antibody-labelled Robo1 levels in the axon and even in the entire neuron were drastically reduced 10 min after

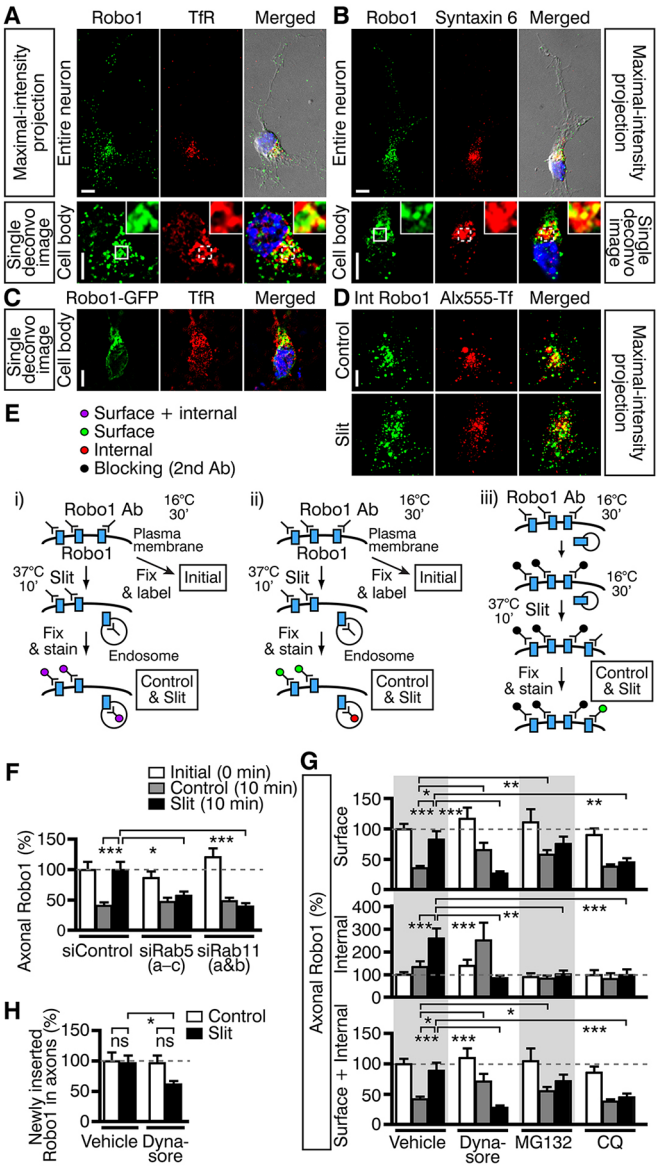

Fig. 2. Slit activates Robo1 endocytic recycling to elevate axonal Robo1 levels. (A-C) Colocalization of endogenous Robo1 (A,B) or Robo1-GFP (C) with TfR (A,C) or syntaxin 6 (B) in E11.5 dorsal spinal cord neurons. Images composed of green (Robo1), red (TfR or syntaxin 6), blue (Hoechst 33342) and DIC channels are shown. (D) Localization of internalized Robo1 and Alexa555-Tf in the commissural neuron cell body. (E) Schematics of live-cell antibody-feeding assays. (i,ii) Monitoring the redistribution of initially surface-located Robo1. Neurons were incubated with anti-Robo1 antibody (Ab) and stimulated with 25 pM Slit for 10 min before detecting both surface and internal Robo1 (i) or separately detecting surface and internal Robo1 (ii) with Alexa-conjugated secondary antibodies. (iii) Monitoring newly surface-inserted Robo1 from intracellular pools. (F) Effects of siRab5 or siRab11 on axonal Robo1 levels. *n*=32-34 neurons (two independent experiments). (G) Quantification of surface, internal and surface+internal levels of antibody-labelled Robo1 in the axon (stained as in Eii). Robo1 levels in the distal-most 30 µm of axons in stimulated neurons were compared with vehicle-treated neurons before stimulation (initial). *n*=76, 76, 77, 61, 60, 59, 45, 45, 46, 47, 47 and 48 neurons (three to five independent experiments). Whether siRab5, siRab11, dynasore, MG132 or CQ significantly suppressed Slit-induced elevation of Robo1 was tested (Mann–Whitney test). **P*<0.05; ***P*<0.01; ****P*<0.0001. (H) Robo1 surface-insertion levels in the axon of neurons stained as in Eiii. *n*=49, 47, 51 and 50 neurons (three independent experiments). ns, not significant. Data are mean±s.e.m. Scale bars: 5 µm in A-D.

Development (2019) 146, dev172106. doi:10.1242/dev.172106

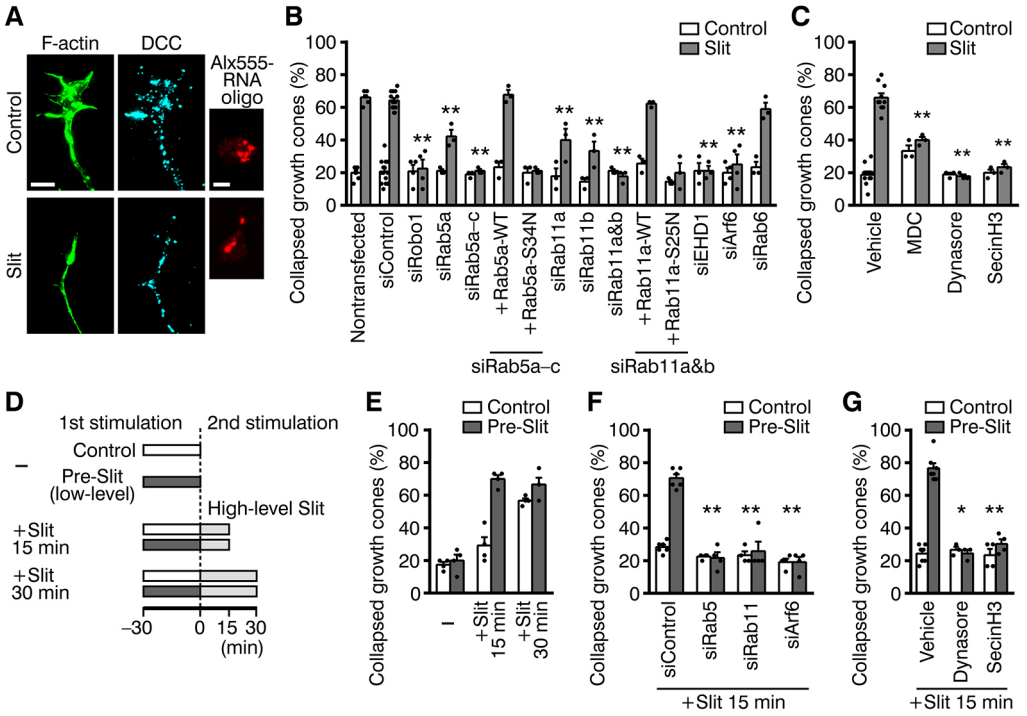

Fig. 3. Both endocytosis and recycling of Robo1 are indispensable for Slit response and sensitization in commissural axons. (A) Growth cone collapse in response to Slit (25 pM, 30 min) in siControl-transfected E11.5 commissural neurons. Growth cone morphology was examined by staining with phalloidin (green) and anti-DCC (cyan). Neurons efficiently transfected with siRNAs were detected by fluorescence of Alexa555-conjugated RNA oligo (red) in the soma and analysed. (B) Quantification of Slit-induced growth cone collapse. *n*=7, 14, 4, 3, 3, 3, 3, 3, 3, 3, 3, 3, 3, 4 and 3 experiments from left to right (30 neurons/experiment). **P*<0.05; ***P*<0.01; Mann–Whitney test. (C) Effects of MDC, dynasore or SecinH3 on Slit responsiveness in E11.5-12.5 commissural neurons. *n*=10, 3, 3 and 3 experiments. (D) Slit sensitization protocols. Pre-stimulated neurons [5 pM Slit (Pre-Slit)] were treated with 25 pM Slit. (E,F) Quantification of Slit-sensitized growth cone collapse in nontransfected (E; *n*=4) and siRNA-transfected (F; *n*=6, 4, 4 and 4) neurons. ***P*=0.0048; Mann–Whitney test. (G) Effects of dynasore or SecinH3 on Slit sensitization. *n*=7, 3 and 4. **P*=0.0167; ***P*=0.003; Mann–Whitney test. Data are mean±s.e.m. Scale bars: 5 µm.

mock-control stimulation [axon: 41.2±5.3% of the initial level (0 min); entire neuron: 41.7±6.2%]. This result indicated that total levels of antibody-labelled Robo1 are not constantly maintained, and suggested that, without Slit, Robo1 that appeared on the surface undergoes a rapid turnover. However, the loss of antibody-labelled Robo1 was effectively blocked by Slit stimulation, leading to a remarkable elevation of Robo1 levels (axon: 100.3±12.9%; entire neuron: 74.0±9.1%). These data confirmed our previous results (Yuasa-Kawada et al., 2009a), suggesting that axonal Robo1 is stabilized by Slit and that mechanisms of Slit-induced Robo1 mobilization are distinct from those of many other ligand-stimulated receptors. Furthermore, in siRab5- or siRab11-transfected neurons, Slit-induced elevation of axonal Robo1 levels was markedly reduced when compared with the siControl group (Fig. 2F). Thus, both endocytosis and recycling are required for Slit-induced elevation of antibody-labelled axonal Robo1 levels.

Next, as shown in Fig. 2Eii, after antibody labelling of surface Robo1 and Slit stimulation, we differentially monitored surface versus internal Robo1 (Fig. S3A). By comparing two immunostaining conditions using unconjugated or Alexa-conjugated secondary antibody before permeabilization (for blocking or detecting of surface Robo1, respectively), we confirmed that internal Robo1 levels could be measured independently of the detection of surface Robo1 (Fig. S3B). In vehicle-treated neurons, antibody labelled axonal Robo1 levels (surface and surface+internal) were reduced during control stimulation [compare initial (0 min) and control (10 min) groups in Fig. 2G and Fig. S4B]. On the other hand, Slit significantly enhanced Robo1 internalization, similar to ligand-induced endocytosis of other receptors. At the same time, Slit blocked the loss of antibody labelled Robo1 [compare initial (0 min) and Slit (10 min) groups in Fig. 2G and Fig. S4B]. These results verified the consistency of differential detection of surface and internal Robo1 (Fig. 2F,G, bottom panel). Initial background levels of internalized Robo1 immediately after antibody labelling (0 min) were 5-10% (Fig. S4C). The internal/(surface+internal) ratios of Robo1, at 10 min after control or Slit stimulation, were similar (e.g. vehicle-treated control-stimulated, 24.6±1.2%; Slit-stimulated, 23.4±1.1%; Fig. S4C), suggesting that surface and internal levels of antibody-labelled Robo1 changed in conjunction with each other, irrespective of Slit stimulation.

We pretreated neurons with dynasore, a dynamin inhibitor that suppresses a number of endocytic pathways (Doherty and McMahon, 2009; Macia et al., 2006). Proteasome inhibitor MG132 and lysosomal inhibitor chloroquine (CQ) were also used. Initial levels of antibody-labelled axonal Robo1 (0 min) were not affected by treatment using these drugs (Fig. 2G). In dynasore-treated neurons without Slit, axon-surface Robo1 levels were higher than those in vehicle-treated neurons (Fig. 2G), suggesting that dynasore-sensitive endocytosis regulates surface Robo1 levels. The same concentration of dynasore blocked Tf uptake, a typical dynamin-dependent endocytic process (Fig. S3C). Strikingly, Slit induced a marked reduction in both surface and internal Robo1 levels in dynasore-treated neurons (Fig. 2G). Western blot analysis showed that total Robo1 levels in dorsal spinal cord neurons were reduced by dynasore treatment, with and without Slit stimulation (Fig. S3D). Together, in dynasore-treated neurons, axon-surface populations of antibody labelled Robo1 were maintained in a steady state, but underwent degradation upon Slit stimulation. Thus,

Development (2019) 146, dev172106. doi:10.1242/dev.172106

dynasore-sensitive endocytic pathways regulated Robo1 transport to the cell-surface during Slit signalling.

The reduction in surface Robo1 levels in the absence of Slit was partially but significantly suppressed by MG132 (Fig. 2G and Fig. S4B), suggesting a role of the ubiquitin-proteasome system in Robo1 degradation under basal conditions. If lysosomal degradation had played a major role in controlling Robo1 levels, CQ should have increased these levels; however, this did not happen (Fig. 2G and Fig. S4B). Thus, lysosomal degradation was not crucial for controlling Robo1 levels.

As shown in Fig. 2Eiii and Fig. S2D, we performed the third type of antibody-feeding assay in commissural neurons, whose surface Robo1 was masked using the anti-Robo1 antibody before stimulation. This experiment allowed us to measure levels of Robo1 proteins that were 'freshly surface inserted' from intracellular pools (Fig. 2H, Figs S3E and S4D). Unexpectedly, levels of freshly surface-inserted Robo1 were not increased upon Slit stimulation, irrespective of dynasore treatment, indicating that surface insertion of intracellularly stored Robo1 made little contribution to Slit-induced elevation of axon-surface Robo1 levels.

Collectively, upon Slit stimulation, substantial fractions of signal-competent Robo1 were endocytosed and recycled back to the cell surface, rather than remaining stagnantly on the surface. These Robo1 endocytosis and recycling cycle(s) happened within 10 min of Slit stimulation. Importantly, inhibition of endocytosis did not elevate surface Robo1 levels, rather it induced Robo1 downregulation in commissural axons, thus supporting the notion that both endocytosis and recycling are required for protecting initially surface-located populations of Robo1 from degradation during Slit signalling and thereby increasing axonal Robo1 levels.

Both endocytic and recycling machineries are indispensable for Slit response and sensitization

To investigate whether Robo1 endocytosis and recycling modulated the Slit sensitivity of commissural neurons, we performed growth cone collapse assays following siRNA-mediated knockdown of specific genes (Fig. 3A,B and Fig. S5A). siControl transfection had no detectable effects on Slit-induced growth cone collapse. Knocking down Robo1 abolished Slit activity in inducing growth cone collapse (Fig. 3B) (Yuasa-Kawada et al., 2009a), indicating that Slit responsiveness of commissural axons is Robo1 mediated. Knockdown of all three Rab5 isoforms, both Rab11 isoforms, Eps15-homology domain protein EHD1 or Arf6, which are all regulators of endocytosis and recycling (Donaldson and Jackson, 2011; Naslavsky et al., 2004; Stenmark, 2009), eliminated Slit sensitivity (Fig. 3B). In contrast, knocking-down Golgi-localized Rab6 did not affect Slit sensitivity. Re-expressing siRNA-resistant wild-type Rab5a or Rab11a, but not their dominant-negative mutants (Rab5a-S34N or Rab11a-S25N), rescued the phenotype induced by siRab5 or siRab11, respectively (Fig. 3B), indicating that the RNAi effects were specific. Our data demonstrated that Rab5 and Rab11 are crucial for the Slit response of commissural neurons. Interestingly, the response of commissural axons to Sema3F, another midline repellent (Zou et al., 2000), was also blocked by siRab5, siRab11 or siArf6 (Fig. S5B). On the other hand, the response of commissural axons to lysophosphatidic acid (LPA), a repellent for axons, was blocked by siRab5, but by neither siRab11 nor siArf6 (Fig. S5C). Thus, endocytic recycling pathways differentially modulate repulsive axonal responses. Similar to a previous study of Slit signalling in *Xenopus* retinal axons (Piper et al., 2006), acute treatment with monodansyl cadaverine (MDC), an inhibitor of clathrin-dependent endocytosis, blocked Slit sensitivity of commissural axons (Fig. 3C). Treatment with dynasore or SecinH3, an inhibitor of cytohesin Arf-GEFs (see below), also abolished the Slit response. Together, these data showed that both endocytic and recycling machineries are essential for Slit response of commissural axons. These data lead us to propose a model for an endocytosis-induced positive-feedback mechanism in Slit-Robo1 signalling (see Fig. 7E). Such a mechanism may enhance Slit sensitivity of commissural axons in response to Slit itself upon midline crossing. This model predicts that repetitive Slit stimulations would augment Slit response of commissural axons, rather than desensitizing them to Slit. To test our model, commissural neurons were first pre-treated with a low dose of Slit and then stimulated with a higher dose of Slit (Fig. 3D). The low level of Slit by itself did not elicit a significant response. However, pre-treatment with low-level Slit markedly enhanced growth cone collapse responses to Slit stimulation at a higher level (Fig. 3E and Fig. S5D). siRab5, siRab11 or siArf6, as well as treatment with dynasore or SecinH3, abolished Slit sensitization (Fig. 3F,G). Therefore, commissural axons are sensitized by Slit in an endocytic recycling-dependent manner that has not been documented previously.

Arf6 is required for elevating Robo1 levels in post-crossing commissural axons

To determine whether this endocytic mechanism played roles in axon midline crossing *in vivo*, we focused on Arf6 signalling, because Arf6 plays important roles in endocytosis and recycling (Donaldson and Jackson, 2011; Yoo et al., 2016; Zhu et al., 2012), and is essential for Slit sensitivity (Fig. 3). We analysed the phenotypes of commissural axons in *Arf6*-deficient mice that were generated in our previous study (Suzuki et al., 2006). Although almost all mice lacking *Arf6* died before birth, post-crossing stage (E12.5) mutants were obtained at a Mendelian ratio, and their gross anatomy appeared normal. Immunohistochemistry confirmed the lack of Arf6 expression in $Arf6^{-/-}$ spinal cords (Fig. S6A). Arf6 was broadly distributed in the spinal cord, with low levels in the midline-crossing commissural axon region. The FP formation was not impaired in $Arf6^{-/-}$ mutants, as shown by FoxA2 expression (Fig. S6B).

We examined whether Robo1 distribution was affected by Arf6 deficiency. In wild-type littermates, Robo1 predominantly localized to the ventral funiculus (VF), post-crossing axon tracts, with low levels being found in pre- and midline-crossing axon segments (Fig. 4A). However, in $Arf6^{-/-}$ mutants, Robo1 immunoreactivity was reduced in the VF and pre-crossing axonal regions (61.6±5.9% of Robo1 levels in the wild-type VF).

We next tested whether axon fibres in the $Arf6^{-/-}$ VF extended from the ipsilateral or contralateral side. We injected DiI into the VF of open-book spinal cords at E12.5 and E14.5, and retrogradely labelled axons and cell bodies (Fig. 4B). In wild-type spinal cords, DiI injection retrogradely labelled commissural axons and their cell bodies on the contralateral side, in addition to ipsilateral axons and commissural axons that extended from the ipsilateral side (anterogradely labelled; Fig. 5C). By contrast, in $Arf6^{-/-}$ spinal cords, the number of retrogradely labelled cell bodies on the contralateral side was significantly reduced (Fig. 4B,D), and instead ipsilateral axons appeared to be dominant. These results suggest that Robo1 immunosignals in the VF were mainly from commissural axons in wild-type mice, but not in $Arf6^{-/-}$ mutants. Robo1 immunosignals in the $Arf6^{-/-}$ VF may have derived from aberrant, ipsilaterally projecting axons.

To determine whether Arf6 regulated Robo1 distribution in post-crossing commissural axons, we prepared spinal cord explants from E11.5 wild-type and $Arf6^{-/-}$ littermates, and examined Robo1

Development (2019) 146, dev172106. doi:10.1242/dev.172106

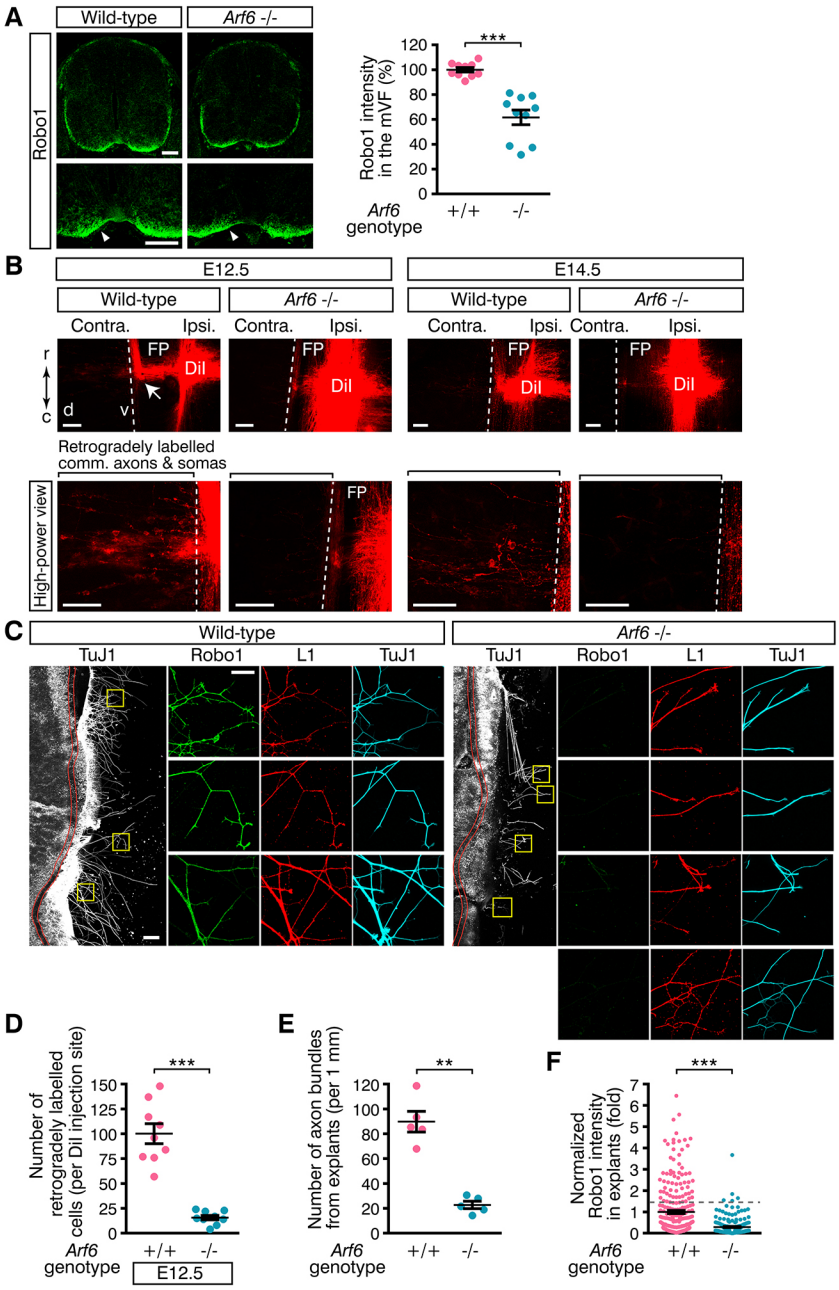

Fig. 4. Arf6 regulates Robo1 distribution in post-crossing commissural axons. (A) Robo1 distribution in E12.5 brachial-level spinal cords (left). The mVF is marked with arrowheads. (Right) Relative Robo1 immunoreactivity in the mVF. *n*=5 (embryos). ***P<0.0001; Mann–Whitney test. (B) Retrograde axon labelling with DiI into the VF in E12.5/E14.5 open-book spinal cords. Dotted lines show the outside edge of the longitudinal axon tract. r, rostral; c, caudal; d, dorsal; v, ventral. (C) Robo1 distribution in post-crossing commissural axons in FP-containing spinal cord explants [SC(+FP)] from E11.5 wild-type and *Arf6*$^{-/-}$ littermates, cultured on Matrigel-precoated coverslips. Triple-immunostaining of explants for Robo1 (green), L1 (red) and TuJ1 (cyan). The FP is marked with red lines. (D) Number of retrogradely labelled cells on the contralateral side to the DiI-injected VF in E12.5 spinal cords, as shown in B (+/+, eight embryos; –/–, nine embryos). ***P<0.0001; Mann–Whitney test. (E) The number of extending axon bundles per 1 mm of SC(+FP) explants from E11.5 wild-type and *Arf6*$^{-/-}$ littermates. *n*=5 (embryos). **P=0.0079; Mann–Whitney test. (F) Robo1 immunoreactivity in the distal axon and axon shaft normalized to TuJ1 immunoreactivity and compared with wild type (stained as in C; eight embryos each; +/+, 261; –/–, 215 imaging fields). ***P<0.0001; Mann–Whitney test. Data are mean±s.e.m. Scale bars: 100 µm in A,B; 200 µm in monochrome images in C; 50 µm in higher magnifications in C.

distribution in commissural axons. Commissural axon extension in *Arf6*$^{-/-}$ dorsal spinal cords was similar to that in wild type (Fig. S6C). However, in FP-containing spinal cords from *Arf6*$^{-/-}$ mutants, reduced numbers of axons crossed the midline (Fig. 4C,E), consistent with *in vivo* findings (see below). Robo1 immunosignals in such post-crossing axons were quantified after normalization to β3-tubulin (TuJ1) signals, which represented axonal density. In *Arf6*$^{-/-}$ explants, there was a marked decrease in Robo1 levels in the distal and shaft parts of L1-positive post-crossing axons (Fig. 4F). Thus, Arf6 regulates Robo1 levels in post-crossing commissural axons.

Roles of Arf6 in commissural axon midline-crossing

TAG-1 immunohistochemistry in wild-type, brachial-level spinal cords revealed an increase in TAG-1 immunoreactivity in the medial part of the VF (mVF) during E11.0-12.5, suggesting that growing commissural axons crossed the midline at these stages (Fig. S7A). TAG-1 immunoreactivity in the mVF was not significantly different between E11.5 and E12.5, indicating that most commissural axons had crossed the midline by E12.5, consistent with previous observations in rats (Altman and Bayer, 1984). We examined commissural axon trajectories in *Arf6*$^{-/-}$ spinal cords at E12.5 by TAG-1 immunostaining. In *Arf6*$^{-/-}$ and *Arf6*$^{+/-}$ mice, commissural axons extended ventrally, similar to wild-type embryos (Fig. 5A). In *Arf6*$^{-/-}$ mutants, however, TAG-1 immunoreactivity was reduced in the mVF to only 32.3% of the wild-type level (Fig. 5A,B). Line-scan profiles of TAG-1 immunofluorescence through the VF and ventral commissure (VC) confirmed a dramatic decrease in TAG-1 immunoreactivity in the *Arf6*$^{-/-}$ VF (Fig. S7B). Similarly, Robo3 immunoreactivity was reduced in the *Arf6*$^{-/-}$ VF (Fig. S7C). These data suggest that many commissural axons were stalled at the midline in *Arf6*$^{-/-}$ mice.

To verify the defects in midline crossing, we traced axon trajectories of commissural neurons in dorsal spinal cords using anterograde DiI labelling. In wild-type embryos, the majority (93.9±0.9%) of commissural axons crossed the FP and made rostral

Development (2019) 146, dev172106. doi:10.1242/dev.172106

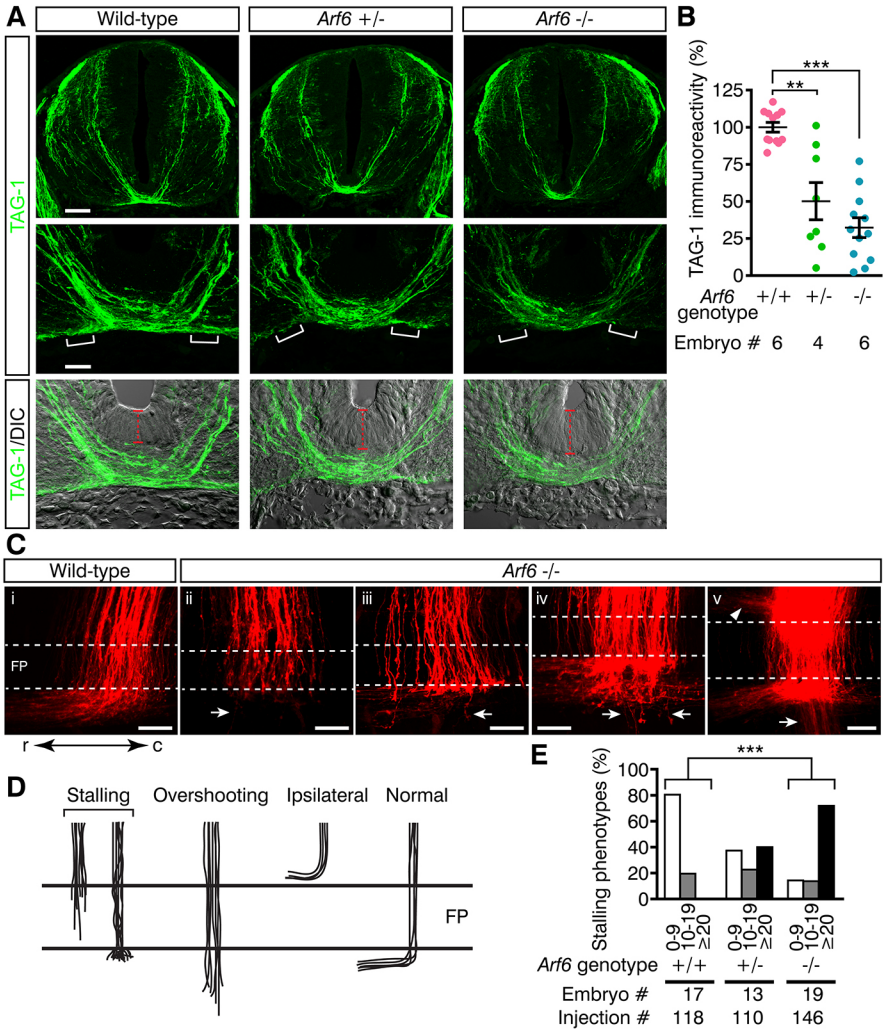

Fig. 5. Defects in axon midline crossing in *Arf6*$^{-/-}$ mutants. (A) TAG-1 immunohistochemistry in E12.5 brachial-level spinal cords. The FP is marked with red dashed lines (bottom panels). (B) Quantification of TAG-1 immunofluorescence in the mVF (marked with white brackets in A). ***P*=0.0093; ****P*<0.0001; Kruskal–Wallis test with Dunn's post-hoc test. (C) Anterograde DiI labelling of dorsal commissural axons in E12.5 open-book spinal cords. (i) Proper axon crossing at the midline in a wild-type embryo. (ii-v) Examples of aberrant axon trajectories in *Arf6*$^{-/-}$ mutants. Axon stalling within the FP and at the contralateral border of the FP, overshooting (arrows) and ipsilaterally turning (arrowhead) were observed. r, rostral; c, caudal. (D) Summary of axonal phenotypes in *Arf6*$^{-/-}$ mutants. (E) Quantification of midline axon stalling (within the FP and at the contralateral FP edge). Percentages of phenotypes showing 0-9, 10-19 or ≥20 stalled axons per DiI injection site are presented as white, grey or black bars, respectively. ****P*<0.0001; χ^2 test. Data are mean±s.e.m. Scale bars: 100 µm in A (top); 25 µm in A (middle and bottom); 50 µm in C.

turns (Fig. 5C). However, remarkable defects were observed in commissural axon midline crossing in *Arf6*$^{-/-}$ mutants with two classes of highly penetrant phenotypes: axon stalling within the FP or at the contralateral FP edge; and axon overshooting into the contralateral side (Fig. 5C,D). The most frequent phenotype was axon stalling at the midline. In 71.9% of DiI-injection sites in *Arf6*$^{-/-}$ mutants, 20 or more axons were stalled within the FP or immediately after exiting, in contrast to wild-type embryos (0%; Fig. 5E). A larger number of axons were stalled at the contralateral FP edge than within the FP (the approximate ratio of 4:1). In addition, in 25.3% of DiI injections in *Arf6*$^{-/-}$ mutants, 10 or more axons showed overshooting into the contralateral side (wild type, 9.3%; Fig. 5C, arrows and Fig. S7E). In 15.1% of DiI injections in dorsal spinal cords in *Arf6*$^{-/-}$ mutants, 10 or more axons turned ipsilaterally (wild type, 0%; Fig. 5C and Fig. S7D,E), suggesting roles for Arf6 in preventing commissural axons from choosing ipsilateral pathways and in enabling midline crossing. DiI tracing of dorso-ventral trajectories of commissural axons revealed clear axon stalling within the FP or at the contralateral FP edge in *Arf6*$^{-/-}$ mutants, with some axons aberrantly entering the contralateral grey matter after crossing (Fig. S7F). Thus, Arf6 is required for midline crossing by commissural axons and their proper midline exit. It should be noted that the axon-stalling phenotype at the midline in *Arf6*$^{-/-}$ mutants was similar to that found in *Robo1*$^{-/-}$ mutants (Jaworski et al., 2010; Long et al., 2004).

Slit-Robo1 signalling involves cytohesin-Arf6 pathways

We examined whether Slit-Robo1 signalling affected Arf6 activity. Arf6-GTP levels were measured in a pulldown assay using glutathione *S*-transferase-fused Golgi-localized gamma-ear-containing Arf-binding protein 1 (GST-GGA1) (Hanai et al., 2016). Slit activated Arf6 in Robo1-expressing HEK293 cells and cortical neurons, but not in control cells lacking Robo1 expression (Fig. 6A,B).

In E12.5 spinal cords, GST-GGA1 detected active Arf GTPases in the midline-crossing axon region of wild-type, but not *Arf6*$^{-/-}$, embryos (Fig. S8A), indicating that Arf6-GTP is the major GTP-bound Arf in E12.5 commissural neurons (GST-GGA1 binds to GTP-bound Arf1-6). GST-GGA1 labelling showed a Slit-induced increase in Arf6 activity in dissociated commissural neurons (Fig. S8B). Various Arf6-GEFs, including cytohesins 1-3 (*Cyth1-Cyth3*), were expressed in dorsal spinal cord neurons (Fig. S8C). Because cytohesins have been implicated in neuronal polarization, with effects similar to Slit-Robo (e.g. Hernández-Deviez et al., 2002; Whitford et al., 2002), we tested whether cytohesins were involved in Slit-Robo signalling. Treatment with cytohesin inhibitor SecinH3 abolished Slit responsiveness and sensitization (Fig. 3), and reduced Slit-induced Arf6 activation in commissural neurons (Fig. S8B), suggesting that Slit-Robo1 signalling activates Arf6 via cytohesins.

To determine which cytohesin member was responsible for Slit signalling, we performed RNAi of Cyth1–Cyth3 in E12.5

Development (2019) 146, dev172106. doi:10.1242/dev.172106

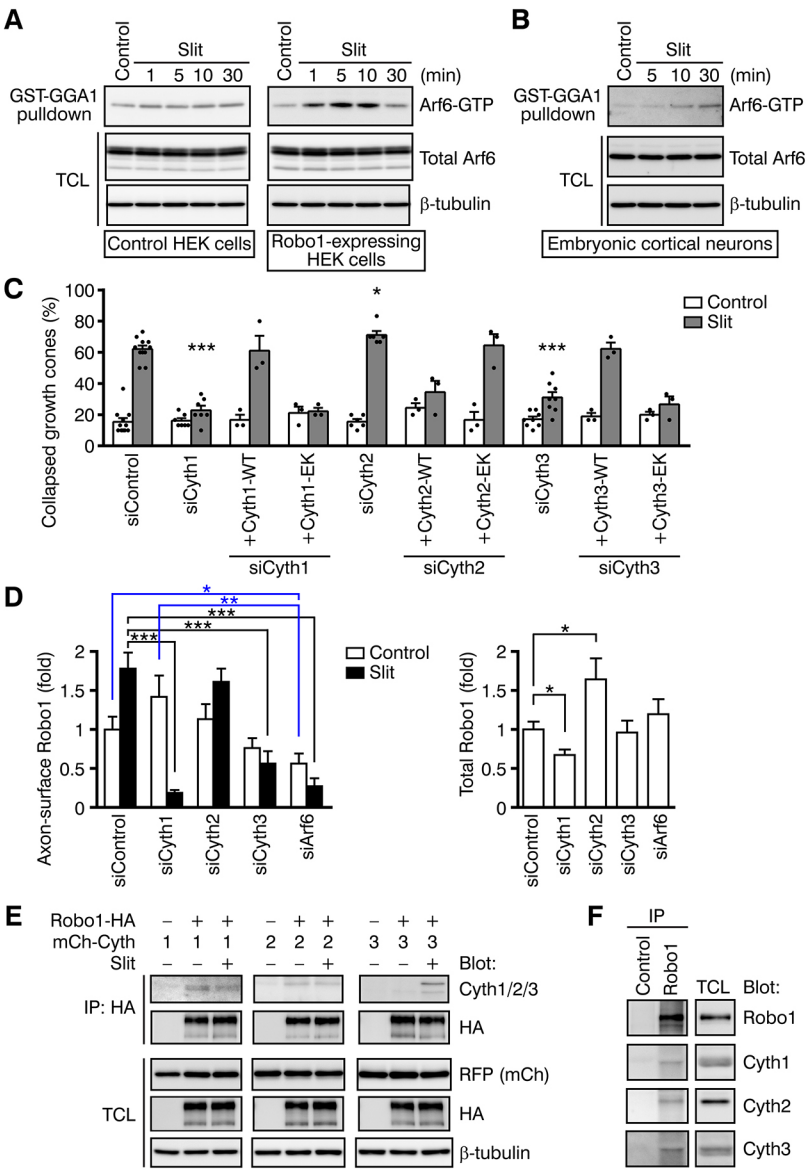

Fig. 6. Cytohesin-Arf6 pathways in Slit-Robo1 signalling. (A) Slit (25 pM) regulation of Arf6 activities in control and Robo1-expressing HEK293 cells transfected with wild-type Arf6 plasmid. Arf6-GTP was captured using GST-GGA1 from total cell lysates (TCL) and detected by immunoblotting with anti-Arf6. (B) Endogenous Arf6 activities in E15.5 cortical neurons stimulated with Slit (25 pM). (C) Quantification of growth cone collapse induced by 25 pM Slit for 30 min in E12.5 commissural neurons transfected with siRNAs to *Cyth1-Cyth3* and with rescue constructs expressing GFP-cytohesins (wild type or EK mutants). *n*=11, 7, 3, 3, 6, 3, 3, 8, 3 and 3 experiments from left to right (30 neurons/experiment). siCyth1 and siCyth3, ***P<0.0001; siCyth2, *P=0.0177; Mann–Whitney test. (D) Effects of RNAi of Cyth1-Cyth3 or Arf6 on axon-surface and total Robo1 levels in E12.5 commissural neurons stimulated with 25 pM Slit for 10 min (three experiments). (Left) *n*=39, 32, 31, 32, 32, 31, 30, 30, 30 and 31 neurons from left to right. Slit-stimulated: siCyth1, siCyth3 and siArf6, ***P<0.0001; Cyth2, P=0.7346 (versus siControl). Control-stimulated: siControl versus siArf6, *P=0.0155. siCyth1 versus siArf6, **P=0.0014. Mann–Whitney test. (Right) *n*=30, 30, 31, 31 and 31 neurons. siCyth1, *P=0.0114; siCyth2, *P=0.0313; siCyth3, P=0.3169; siArf6, P=0.6799. Mann–Whitney test. Data are mean±s.e.m. (E,F) Co-immunoprecipitation of tagged Robo1 and Cyth proteins in HEK293 cells (E) and of endogenous proteins in cell extracts prepared from E16.5 whole brain, including hindbrain and spinal cord (F). In E, cells were stimulated with control preparations (–) or with 25 pM Slit (+) for 5 min. IP, immunoprecipitation.

commissural neurons (Fig. 6C and Fig. S9A-C). Each member has multiple splicing variants with a triglycine (GGG) or diglycine (GG) motif in the pleckstrin homology domain (Ogasawara et al., 2000). GGG/GG motifs differentially affect cytohesin function (Oh and Santy, 2012). We used siRNAs targeting both GGG- and GG-containing cytohesins. Knocking-down Cyth1 or Cyth3 suppressed Slit-induced growth cone collapse. Surprisingly, Cyth2/ARNO knockdown increased the Slit response. These RNAi effects were rescued by re-expressing siRNA-resistant wild-type cytohesins, but not catalytically inactive mutants containing a Glu-to-Lys (EK) substitution in the GEF domain (Fig. 6C). Thus, siRNA-mediated knockdown of cytohesin was specific. In addition, cytohesin GEF activities modulated Slit sensitivity. These results reveal that Cyth1 and Cyth3 are required for Slit response in post-crossing commissural neurons, whereas Cyth2 inhibits Slit response.

To examine the roles of cytohesins and Arf6 in Robo1 endocytic recycling, we measured axon-surface and total Robo1 levels in E12.5 commissural neurons. Although Slit induced an increase in surface Robo1 in siControl-transfected neurons, Cyth1 knockdown led to a reduction in surface Robo1 upon Slit stimulation (Fig. 6D, left). Silencing Cyth3 or Arf6 also suppressed Slit-induced elevation of surface Robo1. Furthermore, axon-surface Robo1 levels were significantly different between siCyth1- and siArf6-transfected neurons without Slit, suggesting that Cyth1 also has Arf6-independent roles in steady-state commissural neurons. In contrast, Cyth2 knockdown did not affect surface Robo1. Robo1 expression in siCyth2-transfected neurons was higher than in control neurons (Fig. 6D, right), suggesting that Cyth2 downregulates Slit signalling by inhibiting Robo1 expression or reducing its stability. Together, Cyth1 and Cyth3, but not Cyth2, mediate Slit-induced Robo1 endocytic recycling and Slit response.

Co-immunoprecipitation showed that Robo1 interacted with Cyth1-Cyth3 in HEK293 cells (Fig. 6E). Slit enhanced Robo1 interaction with Cyth3, but not with Cyth1 or Cyth2. Furthermore, co-immunoprecipitation using Robo1 deletion mutants revealed that Cyth1 interacted with Robo1 CC2 and CC3 motifs (Fig. S8D). Conservation of CC2/3 motifs among Robo1-Robo4 suggests that all Robo proteins may interact with cytohesins. The catalytically inactive mutation of Cyth1 did not affect its interaction with Robo1 (Fig. S8E), indicating that the Robo1-Cyth1 interaction is independent of Cyth1 activity. Interactions between endogenous Robo1 and cytohesins in mouse brain lysates were confirmed

Development (2019) 146, dev172106. doi:10.1242/dev.172106

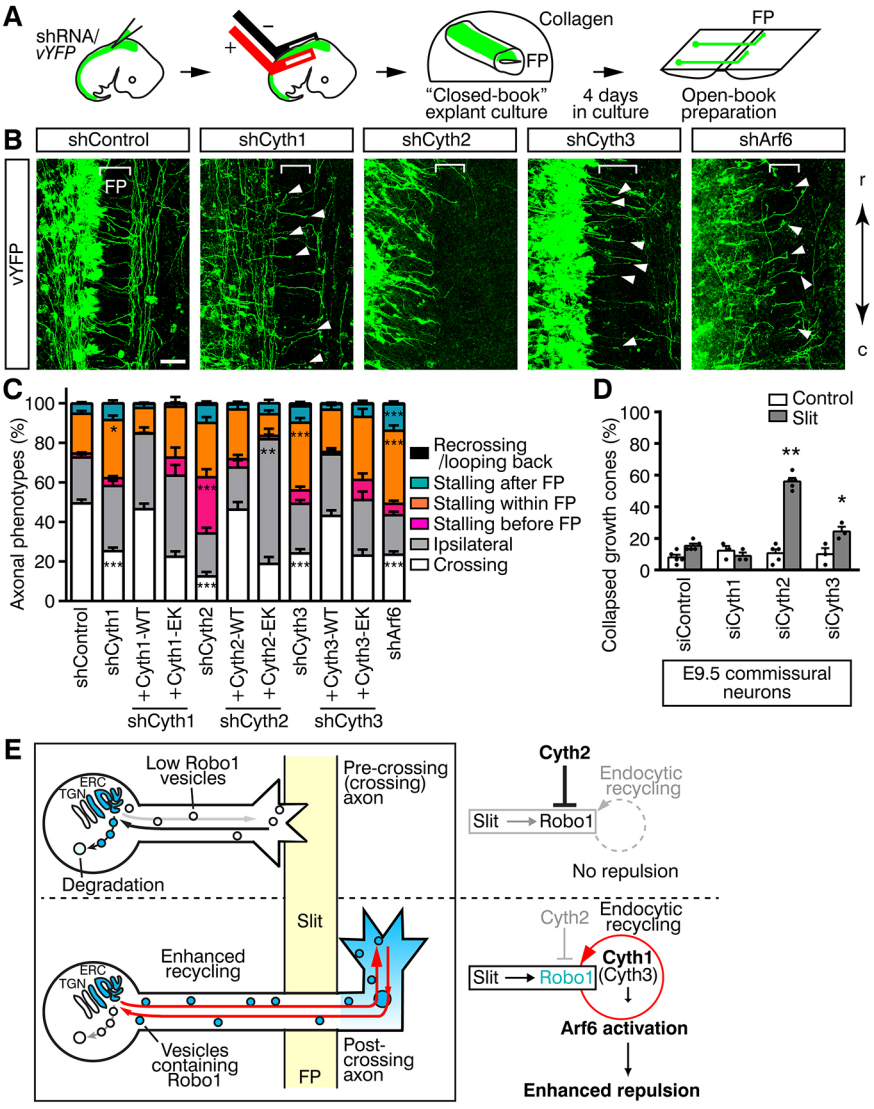

Fig. 7. Roles of cytohesins in commissural axon midline crossing. (A) Protocols for *ex vivo* electroporation and spinal cord explant culture. (B) Midline axon trajectories of *vYFP*- and shRNA-co-electroporated neurons in open-book spinal cords. Axons stalling within the FP (bracket-marked) or at the contralateral FP edge are marked with arrowheads. r, rostral; c, caudal. (C) Quantification and classification of defects in midline axon pathfinding. *n*=91, 44, 18, 17, 46, 11, 16, 33, 16, 21 and 45 (imaging fields) from left to right. **P*<0.05; ***P*<0.01; ****P*<0.001 (versus shControl); Kruskal–Wallis test with Dunn's post-hoc test (at least four embryos analysed per experimental group). (D) Quantification of growth cone collapse induced by 25 pM Slit for 30 min in E9.5 commissural neurons. *n*=5, 3, 5 and 3 experiments from left to right (30 neurons/experiment). Cyth1, *P*=0.1429; Cyth2, ***P*=0.0079; Cyth3, **P*=0.0457; Mann–Whitney test. Data are mean ±s.e.m. (E) Models for midline switching of Slit sensitivity of vertebrate commissural axons. Robo1 endocytosis and recycling cycles constitute a Slit-induced, positive-feedback mechanism for Slit sensitization. This positive-feedback for Slit repulsion is suppressed by Cyth2 before midline crossing, but it is mediated by Cyth1 to allow an axon to cross and exit the FP, thereby generating an endocytic switch in Slit responsiveness. Scale bar: 50 µm.

(Fig. 6F), supporting the hypothesis that cytohesins play roles in Slit-Robo signalling.

Immunostaining of spinal cords showed that Cyth1 and Cyth2 were expressed in the VC (Fig. S9E; for the antibody specificity, see Fig. S9C,D), suggesting the involvement of Cyth1 and Cyth2 in commissural axon midline crossing.

Cytohesin-Arf6 pathways modulate axon midline crossing

To investigate the roles of cytohesins in axon midline crossing, we performed *ex vivo* RNAi in mouse spinal cords (Parra and Zou, 2010). We used two independent sequences of short-hairpin RNAs (shRNAs) targeting both GGG- and GG-type cytohesins and two shRNAs against *Arf6* (Fig. S10A-D). shRNA-encoding constructs, together with a *Venus-YFP* (vYFP, venus-yellow fluorescent protein) plasmid, were co-electroporated unilaterally into dorsal-half regions of E11.5 spinal cords, allowing us to mark shRNA-expressing cells. The spinal cord explants were cultured in collagen gel and examined for axon trajectories (Fig. 7A). In shControl-electroporated spinal cords, we measured vYFP-labelled commissural and ipsilaterally turning axons: 49% of vYFP-positive axons crossed the FP, turning contralaterally in the rostro-caudal direction (Fig. 7B,C). Co-electroporation of *vYFP*-plasmid and shRNAs against cytohesins or *Arf6* into spinal cords led to comparable levels of vYFP expression with those in shControl-targeted spinal cords, and the numbers of vYFP-positive ventrally extending axons were unaffected.

However, in shCyth1-, shCyth3- or shArf6-targeted spinal cords, many vYFP-positive axons were stalled within the FP (including longitudinal axon growth within the FP) or immediately after exiting the FP, whereas in shCyth2-targeted spinal cords, a significant percentage of axons were stalled before entering the FP (Fig. 7B,C and Fig. S10F). Re-crossing was rarely observed. Importantly, such midline-crossing defects were rescued by co-introducing plasmids expressing shRNA-resistant wild-type cytohesins, but not inactive EK mutants (Fig. 7C), thus revealing the specificity of the RNAi and requirements for their Arf-GEF activities in axon midline crossing. Co-introducing *Cyth2-E156 K* mutant plasmid with shCyth2 led to a marked increase in the number of ipsilaterally turning axons (Fig. 7C and Fig. S10E), suggesting that strong suppression of Cyth2 by both RNAi and its dominant-negative mutant prevents midline crossing by commissural axons, leading to their premature ipsilateral turning.

These results prompted us to test whether Cyth2 repressed Slit responsiveness of pre-crossing commissural axons. siControl-transfected E9.5 neurons exhibited negligible Slit sensitivity (Fig. 7D). However, silencing Cyth2, but not Cyth1, enhanced

Development (2019) 146, dev172106. doi:10.1242/dev.172106

Slit sensitivity of E9.5 neurons to a level similar to that in E11.5-12.5 neurons (Fig. 7D). These experiments suggest that removing the inhibitory effects of Cyth2 was sufficient for pre-crossing stage neurons to acquire Slit responsiveness. siCyth3-transfected neurons exhibited a modest level of Slit sensitivity. Together, cytohesin-Arf6 pathways differentially regulate Slit sensitivity in commissural axons before and after midline crossing.

DISCUSSION

Endocytosis is a major mechanism attenuating ligand-induced signalling by removing receptors from the cell surface. In addition, endocytosis modulates the intensity, duration and subcellular distribution of signalling (Cosker and Segal, 2014; Irannejad et al., 2015). We showed that Robo1 endocytosis and recycling are required for Slit response and further sensitization in vertebrate commissural axons upon midline crossing.

Endocytosis and exocytosis/recycling regulate responses of developing axons to guidance cues (Piper et al., 2005; Tojima et al., 2007, 2010). The balance between endocytosis and exocytosis across the growth cone has been implicated in directional axon growth. We found that both endocytic and exocytic/recycling machineries are essential for Slit-induced growth cone collapse. Furthermore, repetitive stimulation with Slit sensitizes, rather than desensitizes, commissural axons, adding another layer of complexity in axon guidance.

We have previously shown that Slit induces elevation of Robo1 surface presentation in cancer cells (Yuasa-Kawada et al., 2009b). The present study has addressed how Robo1 trafficking is regulated in commissural axons. It has been previously reported that Rab guanine nucleotide dissociation inhibitor (RabGDI) and calsyntenin 1, a linker between vesicles and kinesin, promote Robo1 insertion from Rab11-positive recycling compartments to the cell surface and are required for axon midline crossing (Alther et al., 2016; Philipp et al., 2012), consistent with our data. RabGDI recycles GDP-bound Rab proteins from membranes for the next round of Rab activation (Stenmark, 2009). Because Rab11 and Arf6 regulate exocyst complex in polarized exocytosis/recycling (He and Guo, 2009), both RabGDI, as a Rab11 regulator, and Arf6 may mediate Slit-induced elevation of axon-surface Robo1.

We found that axon-surface Robo1 pools are subject to degradation under basal conditions, whereas surface-located Robo1 undergo cycle(s) of endocytosis and recycling upon Slit stimulation; these pools constitute major fractions of axonal Robo1 that are increased by Slit signals in post-crossing neurons. Thus, our study reveals a new mechanism by which the sensitivity of commissural axons to a ligand is enhanced by receptor endocytosis-recycling cycles. It has been proposed that endosomes act as a signalling platform (Scita and Di Fiore, 2010; Villaseñor et al., 2016). We demonstrated that Arf6 signalling is required for Slit sensitization in commissural axons. Furthermore, Arf6-dependent endocytic trafficking of receptors may provide an effective signal-amplification mechanism for axonal responses to midline guidance cues such as Slit and Wnt (Onishi et al., 2013; this study). Another study revealed that, in sympathetic neurons, NGF-mediated stimulation increases surface expression of p75 neurotrophin receptor (p75NTR) via Arf6 activation, thus shifting the responsiveness of TrkA receptor from NT-3 to NGF (Hickman et al., 2018). Therefore, Arf6-based endosomal trafficking pathways may underlie versatile systems for spatiotemporal control of sensitivity to various ligands.

We found that Slit-Robo1 signalling activates Arf6 via cytohesins. Our data support a model in which functionally distinct cytohesin-Arf6 pathways constitute a basic regulatory mechanism for midline switching of Slit sensitivity (Fig. 7E). Cyth2 suppresses Slit repulsion before reaching the midline, enabling axons to enter the midline, whereas Cyth1 mediates Robo1 recycling in response to Slit, allowing axons to cross and exit the midline. These functionally distinct cytohesin-Arf6-based pathways negatively and positively regulate the self-enhancement of Slit response before and after axon midline crossing, respectively, generating a switch in Slit responsiveness.

Although Slit-Robo1 signalling activates Arf6 in commissural neurons, Slit-Robo4 signalling suppresses Arf6 activity in endothelial cells (Jones et al., 2009). Cdc42 and RhoA have been identified as targets for Slit-Robo1 signalling in neurons and cancer cells, respectively (Wong et al., 2001; Kong et al., 2015). Slit may induce a range of diverse responses in different cell types by regulating activities of different GTPases via distinct Robo receptors (Blockus and Chédotal, 2016).

Schizo, another Arf6-GEF, is required for commissure formation in *Drosophila* (Önel et al., 2004). Schizo and Arf6 antagonize Slit signalling in midline cells through endocytosis-mediated inhibition of Slit presentation. In *schizo* mutants, reduced numbers of commissural axons crossed the midline; the other axons avoided entering the midline and possibly undertook ipsilateral routes. A similar Arf6-based mechanism might be involved in midline axon guidance in vertebrates. Our analyses showed that, in *Arf6*$^{-/-}$ mutants, many commissural axons were able to enter the FP but became stalled at the midline, whereas the other populations of commissural axons presumably pursued ipsilateral routes. In shArf6-electroporated dorsal spinal cords, significant populations of axons were stalled at the midline, supporting the notion that Arf6 signalling is required for axon midline crossing in vertebrates. It is tempting to hypothesize that Arf6-based evolutionarily conserved mechanisms specify axonal fate by their selection of commissural or ipsilateral routes.

In *Drosophila*, Robo1 endocytosis from the axon surface, but not its recycling back to the surface, positively regulates Slit repulsion during midline crossing; Robo trafficking into late endosomes induces Robo activation, recruiting its downstream target son of sevenless (Sos) (Chance and Bashaw, 2015). Our data reveal that roles of receptor endocytic trafficking in controlling Slit response are conserved in vertebrates and *Drosophila*, even though the specific molecular players are less conserved. It will be interesting to examine whether vertebrates have acquired the ability to enhance Slit repulsion during axon midline crossing by regulating recycling pathways in an Arf6-dependent manner.

Our study uncovered an Arf6-mediated, cell-intrinsic mechanism that modulates Slit sensitivity, while two extrinsic mechanisms were reported to regulate axonal sensitivity to the other midline repellents Sema3B and Sema3F. Shh attracts commissural axons toward the midline, but also acts as an on-switch cue that enhances the Sema3B/3F response upon midline crossing by suppressing protein kinase A (Parra and Zou, 2010). The protease calpain prevents expression of the Sema receptor plexin A1 in pre-crossing axons. A midline cue, GDNF, and the midline cell-adhesion molecule NrCAM act as on switches that increase axonal plexin-A1 levels by suppressing calpain (Charoy et al., 2012; Nawabi et al., 2010). Importantly, mice that carry mutations in genes encoding various components in Slit and semaphorin signalling pathways exhibit similar axon-pathfinding defects, including axon stalling at the midline. Our results (Fig. S5B) suggest that Arf6 has a general role in repulsive axon guidance at the midline. Accumulating evidence has shown that commissural axons switch Shh responses from attraction to repulsion upon midline crossing (Bourikas et al., 2005; Yam et al., 2012). Furthermore, post-crossing axons are

Development (2019) 146, dev172106. doi:10.1242/dev.172106

repelled rostrally by a caudal-high/rostral-low Shh gradient, and 14-3-3 adaptor proteins are commissural neuron specific, time-dependent switch molecules that drive the attraction-to-repulsion conversion of axonal responses (Yam et al., 2012). It will be interesting to study how Arf6 and 14-3-3 coordinate axon growth during/after midline crossing. Multiple intrinsic and extrinsic mechanisms may generate robust switches in axonal sensitivity to various guidance cues, ensuring that axon crossing at the midline takes place only once.

Coupling spatiotemporally regulated inhibition to a positive-feedback mechanism suggests the existence of a bistable switch in Slit repulsion during axon midline crossing. Mathematical approaches have shown that bistable switches are used in biological processes, including cell fate decision (Ferrell and Xiong, 2001). The midline switch in commissural axons has two major features: the all-or-none response (on/off states of Slit responsiveness) and irreversibility (the one-time off-to-on transition only), both of which are characteristic of a bistable response. Bistability may lead to acquiring responsiveness to guidance cues at an appropriate time and location, and could provide a memory mechanism for neuronal sensitivity to guidance cues, thus generating fidelity and irreversibility of decision-making in axon guidance. We propose that functionally distinct cytohesin-Arf6 pathways contribute to a bistable switch in Slit response during axon midline crossing.

MATERIALS AND METHODS

Animals

Animal experiments were performed according to protocols approved by the Institutional Animal Care and Use Committees (IACUC) of Northwestern University, OIST and Kyushu University. For further details, see the supplementary Materials and Methods.

Antibodies, DNA constructs and reagents

The antibodies, plasmids and reagents used in this study are listed in the supplementary Materials and Methods.

Cell culture and Slit stimulation

Primary neuronal cultures were prepared from E9.5 or E11.5-12.5 dorsal spinal cords, as previously described (Yuasa-Kawada et al., 2009a). HEK293 cells stably expressing human Slit2-myc or rat Robo1-HA were used, as previously described (Li et al., 1999). For further details, see the supplementary Materials and Methods.

Explant culture

Dorsal parts of spinal cords or intact floor plate (FP)-including half parts (from the cervical to lumbar levels) were dissected out from E11.5 embryos and cultured as explants. For further details, see the supplementary Materials and Methods.

siRNAs and shRNAs

To perform RNAi in dissociated, dorsal spinal cord neurons, duplex siRNAs were used. For *ex vivo* electroporation into spinal cords, shRNAs were used. For further details, see the supplementary Materials and Methods.

Live-cell antibody-feeding assays

Different types of live-cell antibody-feeding assays were performed by using our previously published protocol with minor modifications (Yuasa-Kawada et al., 2009a). For further details, see the supplementary Materials and Methods.

Growth cone collapse assays and GST-GGA1 immunolabelling

Slit-, Sema3F- or LPA-stimulated growth cone collapse assays were performed as described previously (Yuasa-Kawada et al., 2009a). For further details, see the supplementary Materials and Methods.

Immunocytochemistry, image acquisition and quantification

Cultured neurons and spinal cord explants were fixed by adding 4% paraformaldehyde (PFA)/10% sucrose in phosphate-buffered saline (PBS) directly to the culture, treated with 50 mM NH_4Cl for 10 min to reduce autofluorescence and permeabilized with 0.2% Triton X-100 in PBS for 5 min. Neurons were then immunolabelled as previously described (Yuasa-Kawada et al., 2009a). Samples were mounted in Permafluor (Thermo Fisher Scientific). For further details on the Immunohistochemistry Method, see the supplementary Materials and Methods.

Z-stacks and time-lapse recordings were acquired using a BX61I microscope (Olympus) with a CoolSNAP HQ or ES CCD camera (Roper Industries). Images were obtained with a PlanApo 60×/NA1.40 oil-immersion objective (Olympus), processed with Leica Deblur or AutoQuant X3 (Media Cybernetics) deconvolution software and analysed using MetaMorph (version 7.7; Molecular Devices). To measure Robo1 signal intensity, DCC^+ neurons were carefully traced (anti-DCC labelled the entire commissural neuron, from the cell body to the axon, irrespective of Slit stimulation) after background signals were subtracted. For quantitative analysis of images, thresholds were set at 3.5-fold background. Integrated signal intensity and the area in the traced region were calculated, and the integrated signal intensity per area or the normalized value was presented in figures. For colocalization analyses (Fig. S2B), the maximal percentage of Robo1-positive pixels overlapping with organelle markers was scored for each set of deconvoluted *z*-stacks. *Z*-stacks of confocal images acquired under LSM710NLO/LSM710, LSM780 (Carl Zeiss) or TCS SP8 (Leica Microsystems) laser-scanning microscope were directly subjected to quantification using MetaMorph.

Images shown in Figs 1-3 were acquired using an Olympus BX61I epifluorescence microscope and deconvoluted. Images in Fig. 4A,C, Fig. 5 and Fig. 7 were acquired using a Zeiss LSM780 confocal microscope. Images in Fig. 4B were acquired using a Zeiss LSM710 confocal microscope.

DiI labelling

Open-book preparations or vibratome sections of spinal cords of E12.5-14.5 wild-type and *Arf6*$^{-/-}$ embryos were injected with DiI (Thermo Fisher Scientific) and the DiI was allowed to diffuse for 2-3 days to label commissural axons along their entire length. For further details, see the supplementary Materials and Methods.

Cell-surface biotinylation, Arf6 pulldown assays, co-immunoprecipitation and western blotting

Biochemical experiments were performed essentially as described previously (Hanai et al., 2016; Yuasa-Kawada et al., 2009a, 2009b). For further details, see the supplementary Materials and Methods.

RT-PCR

Total RNA was extracted from cultured dorsal spinal cord neurons from E11.5 embryos. cDNAs were synthesized by reverse transcription and subjected to PCR. Primers are listed in Table S1. For further details, see the supplementary Materials and Methods.

Ex vivo electroporation and spinal cord explant culture

Spinal cords of E11.5 embryos were injected with shRNA and pCAG-vYFP, and electroporated using NEPA21 (NEPA GENE). The spinal cords were cultured in collagen matrix and subjected to axon trajectory analyses. For further details, see the supplementary Materials and Methods.

Statistical analysis

No statistical methods were used to predetermine sample size. Sample sizes were chosen based on previous experience to obtain statistical significance and reproducibility. Normal distribution of data was not assumed. No data points were excluded, and all data collected from each individual experiment were used for analysis. We noted that axonal phenotypes in commissural neurons varied remarkably along the rostro-caudal axis and on the left/right sides even within the same mouse embryo (Fig. 7). Thus, values quantified on both sides of spinal cords at different rostro-caudal levels of individual embryos were analysed as distinct data points and considered as biological

replicates. Statistical analysis was performed using two-tailed Mann–Whitney, χ^2 or Kruskal–Wallis tests (Prism 6.04 software, GraphPad). For multiple comparisons, Dunn's post-hoc test (after Kruskal–Wallis test) was used. $P<0.05$ was considered statistically significant.

Acknowledgements
We thank J. Bonifacino, S. Bourgoin, S. Caplan, M. Ehlers, J. Gruenberg, J. Ikenouchi, F. Maxfield, F. Murakami, K. Nakayama, A. Tamada and M. Zerial for reagents, and M. Hiramoto for comments. We are grateful to T. Watanabe, K. Iwasaki, Y. Kubota, D. Kang, M. Nomura and W. McGee for support. We also thank three anonymous reviewers for their contributions to the manuscript.

Competing interests
The authors declare no competing or financial interests.

Author contributions
Conceptualization: J.Y.-K., M.K.-K., Y.R., J.Y.W.; Methodology: J.Y.-K., M.K.-K., Y.K., X.C.; Validation: J.Y.-K., M.K.-K., Y.R., J.Y.W.; Formal analysis: J.Y.-K., M.K.-K.; Investigation: J.Y.-K., M.K.-K., H.H.; Resources: T.H., S.Y., Y.K., J.Y.W.; Data curation: J.Y.-K., M.K.-K.; Writing - original draft: J.Y.-K., M.K.-K., Y.R., J.Y.W.; Writing - review & editing: J.Y.-K., M.K.-K., Y.R., J.Y.W.; Visualization: J.Y.-K., M.K.-K.; Supervision: J.Y.-K., Y.R., J.Y.W.; Project administration: J.Y.-K., T.M., Y.R.; Funding acquisition: J.Y.-K., I.M., Y.T., J.Y.W.

Funding
This work was supported by grants from the Japan Society for the Promotion of Science (24570245 to J.Y.-K.), the Okinawa Institute of Science and Technology (to I.M.) and the National Institutes of Health (R01CA175360 to J.Y.W.). Deposited in PMC for release after 12 months.

Supplementary information
Supplementary information available online at
http://dev.biologists.org/lookup/doi/10.1242/dev.172106.supplemental

References
Alther, T. A., Domanitskaya, E. and Stoeckli, E. T. (2016). Calsyntenin 1-mediated trafficking of axon guidance receptors regulates the switch in axonal responsiveness at a choice point. *Development* **143**, 994-1004.
Altman, J. and Bayer, S. A. (1984). The development of the rat spinal cord. *Adv. Anat. Embryol. Cell Biol.* **85**, 1-164.
Blockus, H. and Chédotal, A. (2016). Slit-Robo signaling. *Development* **143**, 3037-3044.
Bock, J. B., Klumperman, J., Davanger, S. and Scheller, R. H. (1997). Syntaxin 6 functions in trans-Golgi network vesicle trafficking. *Mol. Cell Biol.* **8**, 1261-1271.
Bourikas, D., Pekarik, V., Baeriswyl, T., Grunditz, A., Sadhu, R., Nardó, M. and Stoeckli, E. T. (2005). Sonic hedgehog guides commissural axons along the longitudinal axis of the spinal cord. *Nat. Neurosci.* **8**, 297-304.
Brose, K., Bland, K. S., Wang, K. H., Arnott, D., Henzel, W., Goodman, C. S., Tessier-Lavigne, M. and Kidd, T. (1999). Slit proteins bind Robo receptors and have an evolutionarily conserved role in repulsive axon guidance. *Cell* **96**, 795-806.
Chance, R. K. and Bashaw, G. J. (2015). Slit-dependent endocytic trafficking of the Robo receptor is required for Son of Sevenless recruitment and midline axon repulsion. *PLoS Genet.* **11**, e1005402.
Charoy, C., Nawabi, H., Reynaud, F., Derrington, E., Bozon, M., Wright, K., Falk, J., Helmbacher, F., Kindbeiter, K. and Castellani, V. (2012). Gdnf activates midline repulsion by Semaphorin3B via NCAM during commissural axon guidance. *Neuron* **75**, 1051-1066.
Chen, Z., Gore, B. B., Long, H., Ma, L. and Tessier-Lavigne, M. (2008). Alternative splicing of the Robo3 axon guidance receptor governs the midline switch from attraction to repulsion. *Neuron* **58**, 325-332.
Cosker, K. E. and Segal, R. A. (2014). Neuronal signaling through endocytosis. *Cold Spring Harb. Perspect. Biol.* **6**, a020669.
Dodd, J., Morton, S. B., Karagogeos, D., Yamamoto, M. and Jessell, T. M. (1988). Spatial regulation of axonal glycoprotein expression on subsets of embryonic spinal neurons. *Neuron* **1**, 105-116.
Doherty, G. J. and McMahon, H. T. (2009). Mechanisms of endocytosis. *Annu. Rev. Biochem.* **78**, 857-902.
Donaldson, J. G. and Jackson, C. L. (2011). ARF family G proteins and their regulators: roles in membrane transport, development and disease. *Nat. Rev. Mol. Cell Biol.* **12**, 362-375.
Ducuing, H., Gardette, T., Pignata, A., Tauszig-Delamasure, S. and Castellani, V. (2018). Commissural axon navigation in the spinal cord: a repertoire of repulsive forces is in command. *Semin. Cell Dev. Biol.* **85**, 3-12.
Ferrell, J. E. Jr. and Xiong, W. (2001). Bistability in cell signaling: how to make continuous processes discontinuous, and reversible processes irreversible. *Chaos* **11**, 227-236.
Guan, K.-L. and Rao, Y. (2003). Signalling mechanisms mediating neuronal responses to guidance cues. *Nat. Rev. Neurosci.* **4**, 941-956.
Hanai, A., Ohgi, M., Yagi, C., Ueda, T., Shin, H.-W. and Nakayama, K. (2016). Class I Arfs (Arf1 and Arf3) and Arf6 are localized to the Flemming body and play important roles in cytokinesis. *J. Biochem.* **159**, 201-208.
He, B. and Guo, W. (2009). The exocyst complex in polarized exocytosis. *Curr. Opin. Cell Biol.* **21**, 537-542.
Hernández-Deviez, D. J., Casanova, J. E. and Wilson, J. M. (2002). Regulation of dendritic development by the ARF exchange factor ARNO. *Nat. Neurosci.* **5**, 623-624.
Hickman, F. E., Stanley, E. M. and Carter, B. D. (2018). Neurotrophin responsiveness of sympathetic neurons is regulated by rapid mobilization of the p75 receptor to the cell surface through TrkA activation of Arf6. *J. Neurosci.* **38**, 5606-5619.
Irannejad, R., Tsvetanova, N. G., Lobingier, B. T. and von Zastrow, M. (2015). Effects of endocytosis on receptor-mediated signaling. *Curr. Opin. Cell Biol.* **35**, 137-143.
Jaworski, A., Long, H. and Tessier-Lavigne, M. (2010). Collaborative and specialized functions of Robo1 and Robo2 in spinal commissural axon guidance. *J. Neurosci.* **30**, 9445-9453.
Jones, C. A., Nishiya, N., London, N. R., Zhu, W., Sorensen, L. K., Chan, A. C., Lim, C. J., Chen, H., Zhang, Q., Schulz, P. G. et al. (2009). Slit2-Robo4 signalling promotes vascular stability by blocking Arf6 activity. *Nat. Cell Biol.* **11**, 1325-1331.
Justice, E. D., Barnum, S. J. and Kidd, T. (2017). The WAGR syndrome gene PRRG4 is a functional homologue of the commissureless axon guidance gene. *PLoS Genet.* **13**, e1006865.
Keino-Masu, K., Masu, M., Hinck, L., Leonardo, E. D., Chan, S. S.-Y., Culotti, J. G. and Tessier-Lavigne, M. (1996). Deleted in Colorectal Cancer (DCC) encodes a netrin receptor. *Cell* **87**, 175-185.
Keleman, K., Rajagopalan, S., Cleppien, D., Teis, D., Paiha, K., Huber, L. A., Technau, G. M. and Dickson, B. J. (2002). Comm sorts Robo to control axon guidance at the *Drosophila* midline. *Cell* **110**, 415-427.
Keleman, K., Ribeiro, C. and Dickson, B. J. (2005). Comm function in commissural axon guidance: cell-autonomous sorting of Robo in vivo. *Nat. Neurosci.* **8**, 156-163.
Kidd, T., Russell, C., Goodman, C. S. and Tear, G. (1998). Dosage-sensitive and complementary functions of roundabout and commissureless control axon crossing of the CNS midline. *Neuron* **20**, 25-33.
Kidd, T., Bland, K. S. and Goodman, C. S. (1999). Slit is the midline repellent for the Robo receptor in *Drosophila*. *Cell* **96**, 785-794.
Kolodkin, A. L. and Tessier-Lavigne, M. (2011). Mechanisms and molecules of neuronal wiring: a primer. *Cold Spring Harb. Perspect. Biol.* **3**, a001727.
Kong, R., Yi, F., Wen, P., Liu, J., Chen, X., Ren, J., Li, X., Shang, Y., Nie, Y., Wu, K. et al. (2015). Myo9b is a key player in SLIT/ROBO-mediated lung tumor suppression. *J. Clin. Invest.* **125**, 4407-4420.
Lewis, T. L. Jr., Courchet, J. and Polleux, F. (2013). Cellular and molecular mechanisms underlying axon formation, growth, and branching. *J. Cell Biol.* **202**, 837-848.
Li, H.-S., Chen, J.-H., Wu, W., Fagaly, T., Zhou, L., Yuan, W., Dupuis, S., Jiang, Z.-H., Nash, W., Gick, C. et al. (1999). Vertebrate Slit, a secreted ligand for the transmembrane protein Roundabout, is a repellent for olfactory bulb axons. *Cell* **96**, 807-818.
Long, H., Sabatier, C., Ma, L., Plump, A., Yuan, W., Ornitz, D. M., Tamada, A., Murakami, F., Goodman, C. S. and Tessier-Lavigne, M. (2004). Conserved roles for Slit and Robo proteins in midline commissural axon guidance. *Neuron* **42**, 213-223.
Macia, E., Ehrlich, M., Massol, R., Boucrot, E., Brunner, C. and Kirchhausen, T. (2006). Dynasore, a cell-permeable inhibitor of dynamin. *Dev. Cell* **10**, 839-850.
Maxfield, F. R. and McGraw, T. E. (2004). Endocytic recycling. *Nat. Rev. Mol. Cell Biol.* **5**, 121-132.
Naslavsky, N., Boehm, M., Backlund, P. S. Jr. and Caplan, S. (2004). Robenosyn-5 and EHD1 interact and sequentially regulate protein recycling to the plasma membrane. *Mol. Biol. Cell* **15**, 2410-2422.
Nawabi, H., Briançon-Marjollet, A., Clark, C., Sanyas, I., Takamatsu, H., Okuno, T., Kumanogoh, A., Bozon, M., Takeshima, K., Yoshida, Y. et al. (2010). A midline switch of receptor processing regulates commissural axon guidance in vertebrates. *Genes Dev.* **24**, 396-410.
O'Donnell, M., Chance, R. K. and Bashaw, G. J. (2009). Axon growth and guidance: receptor regulation and signal transduction. *Annu. Rev. Neurosci.* **32**, 383-412.
Ogasawara, M., Kim, S.-C., Adamik, R., Togawa, A., Ferrans, V. J., Takeda, K., Kirby, M., Moss, J. and Vaughan, M. (2000). Similarities in function and gene structure of cytohesin-4 and cytohesin-1, guanine nucleotide-exchange proteins for ADP-ribosylation factors. *J. Biol. Chem.* **275**, 3221-3230.
Oh, S. J. and Santy, L. C. (2012). Phosphoinositide specificity determines which cytohesins regulate β1 integrin recycling. *J. Cell Sci.* **125**, 3195-3201.

Okada, A., Charron, F., Morin, S., Shin, D. S., Wong, K., Fabre, P. J., Tessier-Lavigne, M. and McConnell, S. K. (2006). Boc is a receptor for sonic hedgehog in the guidance of commissural axons. *Nature* **444**, 369-373.
Önel, S., Bolke, L. and Klämbt, C. (2004). The Drosophila ARF6-GEF Schizo controls commissure formation by regulating Slit. *Development* **131**, 2587-2594.
Onishi, K., Shafer, B., Lo, C., Tissir, F., Goffinet, A. M. and Zou, Y. (2013). Antagonistic functions of Dishevelleds regulate Frizzled3 endocytosis via filopodia tips in Wnt-mediated growth cone guidance. *J. Neurosci.* **33**, 19071-19085.
Parra, L. M. and Zou, Y. (2010). Sonic hedgehog induces response of commissural axons to Semaphorin repulsion during midline crossing. *Nat. Neurosci.* **13**, 29-35.
Philipp, M., Niederkofler, V., DEbrunner, M., Alther, T., Kunz, B. and Stoeckli, E. T. (2012). RabGDI controls axonal midline crossing by regulating Robo1 surface expression. *Neural Dev.* **7**, 36.
Piper, M., Salih, S., Weinl, C., Holt, C. E. and Harris, W. A. (2005). Endocytosis-dependent desensitization and protein synthesis-dependent resensitization in retinal growth cone adaptation. *Nat. Neurosci.* **8**, 179-186.
Piper, M., Anderson, R., Dwivedy, A., Weinl, C., van Horck, F., Leung, K. M., Cogill, E. and Holt, C. (2006). Signaling mechanisms underlying Slit2-induced collapse of *Xenopus* retinal growth cones. *Neuron* **49**, 215-228.
Sabatier, C., Plump, A. S., Ma, L., Brose, K., Tamada, A., Murakami, F., Lee, E. Y.-H. P. and Tessier-Lavigne, M. (2004). The divergent Robo family protein Rig-1/Robo3 is a negative regulator of Slit responsiveness required for midline crossing by commissural axons. *Cell* **117**, 157-169.
Scita, G. and Di Fiore, P. P. (2010). The endocytic matrix. *Nature* **463**, 464-473.
Seki, M., Watanabe, A., Enomoto, S., Kawamura, T., Ito, H., Kodama, T., Hamakubo, T. and Aburatani, H. (2010). Human ROBO1 is cleaved by metalloproteinases and gamma-secretase and migrates to the nucleus in cancer cells. *FEBS Lett.* **584**, 2909-2915.
Stenmark, H. (2009). Rab GTPases as coordinators of vesicle traffic. *Nat. Rev. Mol. Cell Biol.* **10**, 513-525.
Stoeckli, E. (2017). Where does axon guidance lead us? *F1000Res* **6**, 78.
Suzuki, T., Kanai, Y., Hara, T., Sasaki, J., Sasaki, T., Kohara, M., Maehama, T., Taya, C., Shitara, H., Yonekawa, H. et al. (2006). Crucial role of the small GTPase ARF6 in hepatic cord formation during liver development. *Mol. Cell Biol.* **26**, 6149-6156.
Tamada, A., Kumada, T., Zhu, Y., Matsumoto, T., Hatanaka, Y., Muguruma, K., Chen, Z., Tanabe, Y., Torigoe, M., Yamauchi, K. et al. (2008). Crucial roles of Robo proteins in midline crossing of cerebellofugal axons and lack of their up-regulation after midline crossing. *Neural Dev.* **3**, 29.
Tojima, T., Akiyama, H., Itofusa, R., Li, Y., Katayama, H., Miyawaki, A. and Kamiguchi, H. (2007). Attractive axon guidance involves asymmetric membrane transport and exocytosis in the growth cone. *Nat. Neurosci.* **10**, 58-66.
Tojima, T., Itofusa, R. and Kamiguchi, H. (2010). Asymmetric clathrin-mediated endocytosis drives repulsive growth cone guidance. *Neuron* **66**, 370-377.
Villaseñor, R., Kalaidzidis, Y. and Zerial, M. (2016). Signal processing by the endosomal system. *Curr. Opin. Cell Biol.* **39**, 53-60.
Whitford, K. L., Marillat, V., Stein, E., Goodman, C. S., Tessier-Lavigne, M., Chédotal, A. and Ghosh, A. (2002). Regulation of cortical dendrite development by Slit-Robo interactions. *Neuron* **33**, 47-61.
Wong, K., Ren, X.-R., Huang, Y.-Z., Xie, Y., Liu, G., Saito, H., Tang, H., Wen, L., Brady-Kalnay, S. M., Mei, L. et al. (2001). Signal transduction in neuronal migration: roles of GTPase activating proteins and the small GTPase Cdc42 in the Slit-Robo pathway. *Cell* **107**, 209-221.
Yam, P. T., Kent, C. B., Morin, S., Farmer, W. T., Alchini, R., Lepelletier, L., Colman, D. R., Tessier-Lavigne, M., Fournier, A. E. and Charron, F. (2012). 14-3-3 proteins regulate a cell-intrinsic switch from sonic hedgehog-mediated commissural axon attraction to repulsion after midline crossing. *Neuron* **76**, 735-749.
Yoo, J. H., Shi, D. S., Grossmann, A. H., Sorensen, L. K., Tong, Z., Mleynek, T. M., Rogers, A., Zhu, W., Richards, J. R., Winter, J. M. et al. (2016). ARF6 is an actionable node that orchestrates oncogenic GNAQ signaling in uveal melanoma. *Cancer Cell* **29**, 889-904.
Yuasa-Kawada, J., Kinoshita-Kawada, M., Wu, G., Rao, Y. and Wu, J. Y. (2009a). Midline crossing and Slit responsiveness of commissural axons require USP33. *Nat. Neurosci.* **12**, 1087-1089.
Yuasa-Kawada, J., Kinoshita-Kawada, M., Rao, Y. and Wu, J. Y. (2009b). Deubiquitinating enzyme USP33/VDU1 is required for Slit signaling in inhibiting breast cancer cell migration. *Proc. Natl. Acad. Sci. USA* **106**, 14530-14535.
Zerial, M. and McBride, H. (2001). Rab proteins as membrane organizers. *Nat. Rev. Mol. Cell Biol.* **2**, 107-117.
Zhu, W., London, N. R., Gibson, C. C., Davis, C. T., Tong, Z., Sorensen, L. K., Shi, D. S., Guo, J., Smith, M. C., Grossmann, A. H. et al. (2012). Interleukin receptor activates a MYD88-ARNO-ARF6 cascade to disrupt vascular stability. *Nature* **492**, 252-255.
Zou, Y., Stoeckli, E., Chen, H. and Tessier-Lavigne, M. (2000). Squeezing axons out of the gray matter: a role for Slit and Semaphorin proteins from midline and ventral spinal cord. *Cell* **102**, 363-375.

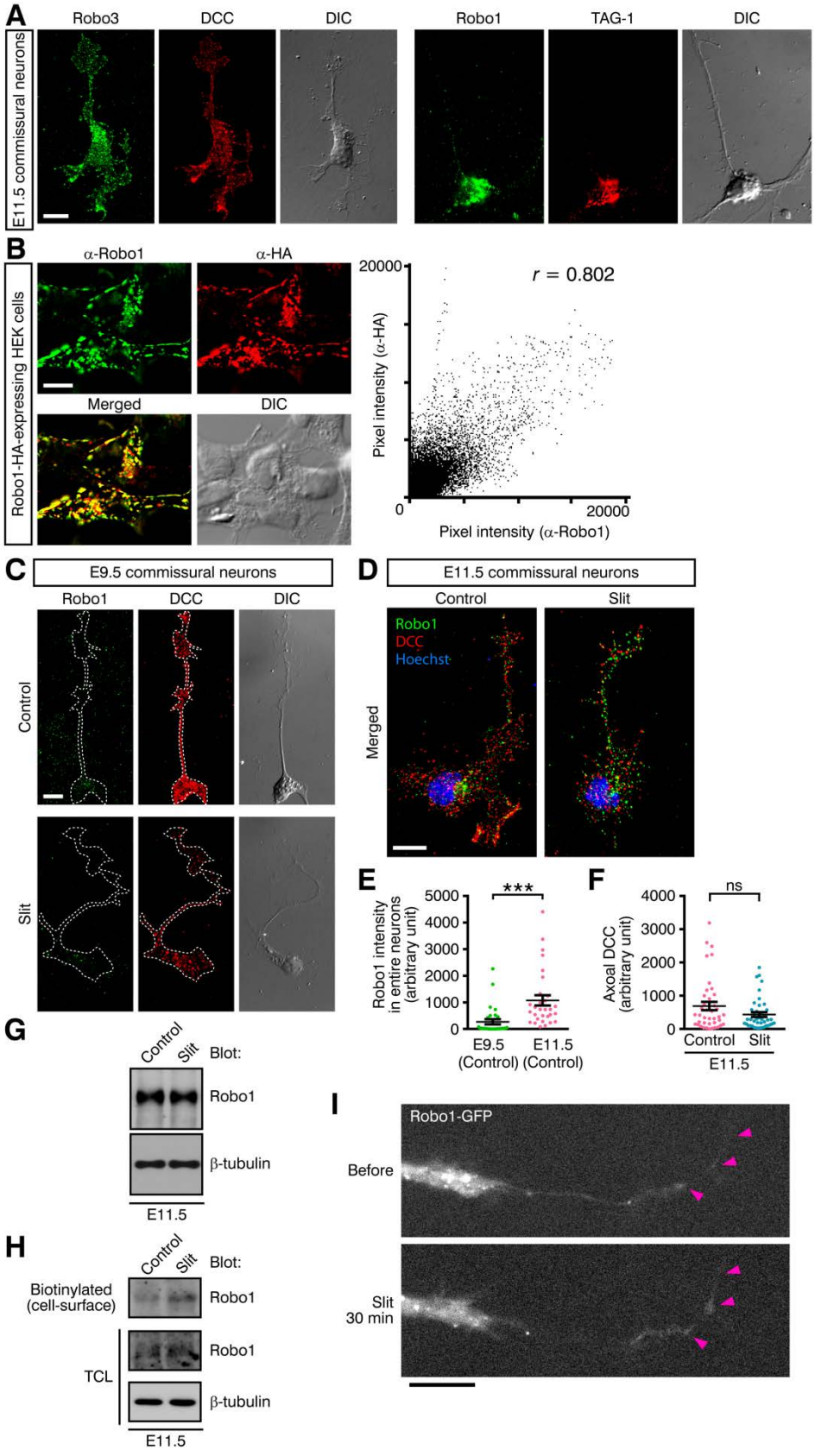

Figure S1. Robo1 expression and dynamics in commissural neurons. (A) Co-immunostaining of Robo3 (green) and DCC (red) (left) or Robo1 (green) and TAG-1 (red) (right) in E11.5 dorsal spinal cord neurons. Differential interference contrast (DIC) images are also shown. (B) Co-immunostaining of Robo1-HA [C-terminally hemagglutinin (HA)-tagged]–expressing HEK293 cells with anti-Robo1 (green) and anti-HA (red) antibodies (left panel). Right panel: spatial pixel intensity correlations between anti-Robo1 and anti-HA signals. Pearson's correlation coefficient (*r*) is shown. (C) Subcellular distribution of Robo1 (green) in E9.5 DCC^+ (red) commissural neurons stimulated with 25 pM Slit for 10 min. The images were taken under the same conditions as in Fig. 1A. (D) The merged images of E11.5 triple-labelled [Robo1 (green)/DCC (red)/Hoechst33342 (blue)] commissural neurons shown in Fig. 1A. A small fraction of Robo1 exhibited an overlap with DCC. (E) Comparison of Robo1 immunosignal intensity per area of the entire neuron between E9.5 and 11.5 DCC^+ commissural neurons stimulated with the control. Here and in subsequent figures, mean ± SEM is presented. $n = 30$ (neurons) (10 neurons/experiment, 3 independent experiments). $^{***}P < 0.001$; two-tailed Mann-Whitney test. (F) DCC levels in the distal axon of commissural neurons stained as in Fig. 1A. $n = 30$ (neurons) (10 neurons/experiment, 3 experiments). $P = 0.2011$; Mann-Whitney test. ns: not significant. (G) Western blot analysis showing Robo1 protein expression in E11.5 dorsal spinal cord neurons stimulated with 25 pM Slit or control for 10 min. The overall levels of Robo1 were not affected by Slit during the time frame of our observation. (H) Cell-surface biotinylation of Robo1 in primary dorsal spinal cord neurons prepared from E12.5 mouse embryos. Neurons were stimulated with 25 pM Slit for 10 min. Extracellular domains were biotinylated for 30 min on ice, and the biotinylated proteins were recovered by pulldown using avidin-agarose and subjected to Western blot analysis. (I) Live-cell imaging of the axon of a Robo1-GFP-expressing dorsal spinal cord neuron cultured from E11.5 embryos. The neuron was imaged before and after Slit stimulation (25 pM). The growth cone is marked with red arrows. Scale bars, 10 μm (A–D,I). All immunofluorescence images were acquired using an Olympus BX61I epifluorescence microscope and deconvoluted. Robo1 and TAG-1 immunostaining images in (A) were denoised using Sefir software before deconvolution.

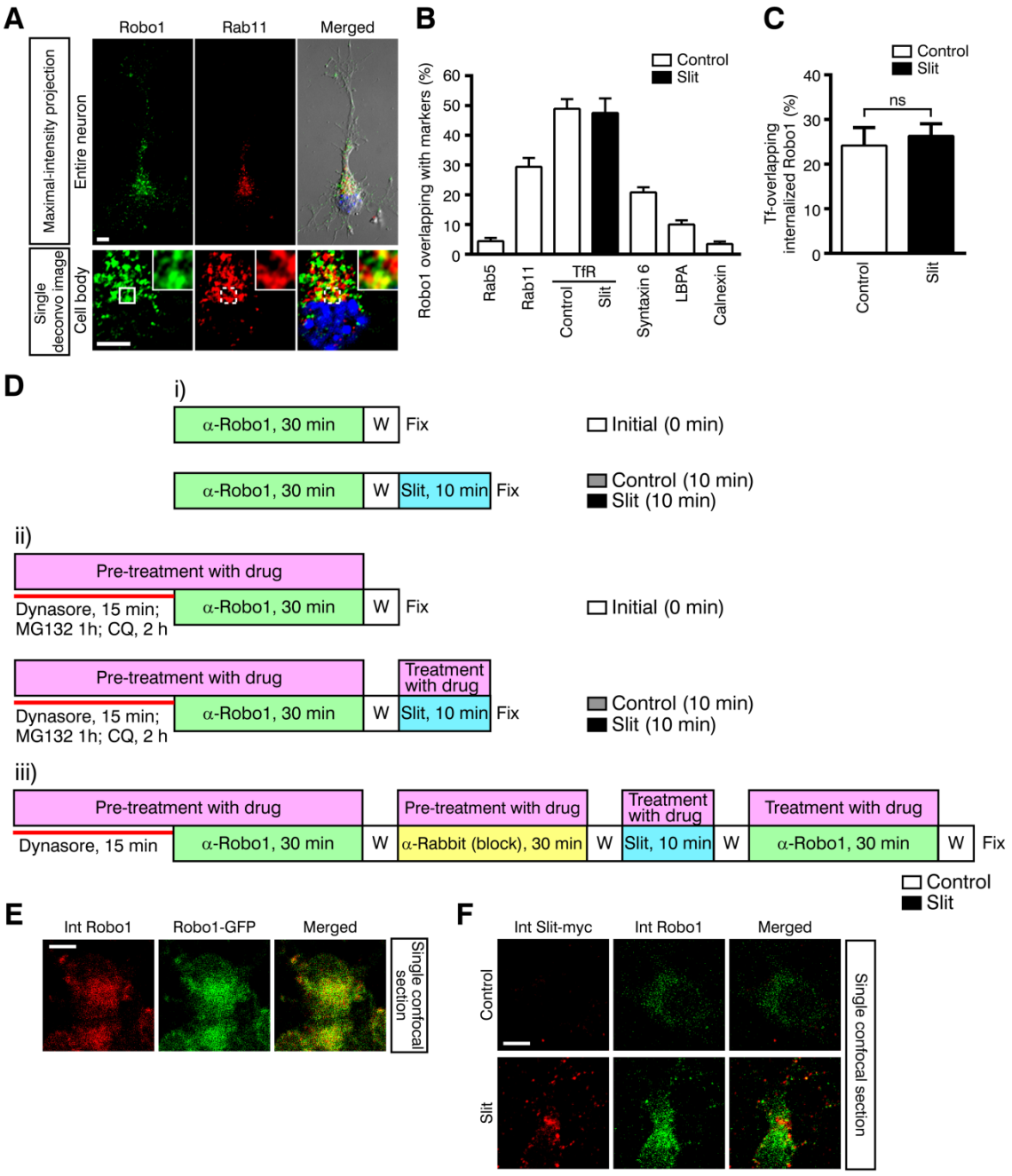

Figure S2. Robo1 localization in the endocytic recycling compartment and schemes of live-cell antibody-feeding assays. (A) Endogenous Robo1 exhibits a partial overlap with Rab11 in E11.5 dorsal spinal cord neurons. Images composed of green (Robo1), red (Rab11), blue (Hoechst 33342) and DIC channels and magnified views are shown. (B) Percentages of Robo1-positive pixels overlapping with organelle markers in the cell body were quantified. Lysobisphosphatidic acid (LBPA) and calnexin were used as markers for late endosomes and the endoplasmic reticulum, respectively. *n* = 10, 10, 11, 11, 11, 10 and 10 (neurons) from left to right. (C) Quantification of percentages of Alexa555-Tf–overlapping, internalized Robo1 in neurons immunostained as in Fig. 2D. *n* = 10

(neurons). $P = 0.4727$; Mann-Whitney test. ns: not significant. (D) Time course of drug treatment and antibody-labelling in antibody-feeding assays shown in Fig. 2E. (E) The distribution of anti-Robo1 antibody (red) internalized after surface-labelling in E12.5 primary dorsal spinal cord neurons expressing Robo1-GFP (green). (F) Slit-binding assay in E12.5 primary dorsal spinal cord neurons. Partially overlapping distribution of internalized Slit2-myc (red, detected with anti-myc) and internalized Robo1 (green). Scale bars, 5 μm (A,E,F). Images in (A) were acquired using an Olympus BX61I epifluorescence microscope and deconvoluted. Images in (E,F) were obtained with a Zeiss LSM710 confocal microscope.

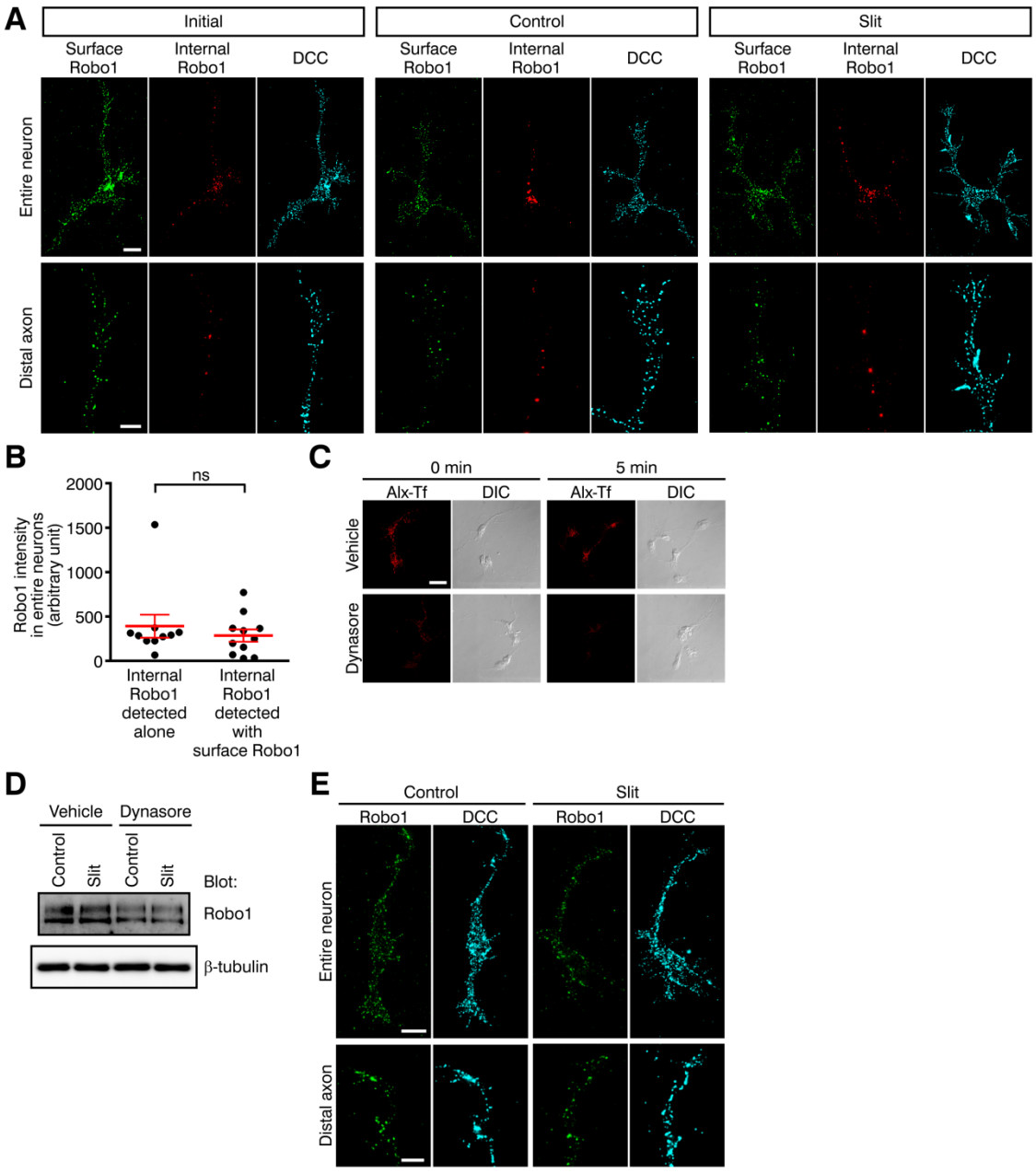

Figure S3. Differential detection of surface, internal and freshly surface-inserted Robo1 in antibody-feeding assays. (A) Robo1 immunostaining in vehicle-treated neurons stained as in Fig. 2E-ii). Maximal-intensity projections of deconvoluted Z-stacks are shown. Neurons were incubated with anti-Robo1 and stimulated with 25 pM Slit or control for 10 min before fixation and differential detection of surface (green) and internal (red) Robo1. DCC expression is shown in cyan. (B) Comparison of signal intensity per area between internal Robo1 levels detected alone and those detected simultaneously with surface Robo1. Both of the internal Robo1 levels were measured in entire neurons that were stimulated with control for 10 min after labelling with anti-Robo1. 'Internal Robo1 levels detected alone' were quantified in the neurons in which surface Robo1 was blocked with unconjugated anti-rabbit secondary antibody. 'Internal

Robo1 levels detected simultaneously with surface Robo1 levels' were quantified in the neurons stained as in Fig. 2E-ii). *n* = 11 (neurons). *P* = 0.6433. ns: not significant. (C) Suppression of Tf uptake in commissural neurons by treatment with dynasore. Maximal-intensity projections of deconvoluted Z-stacks together with DIC images are shown. Neurons were treated with 40 μM dynasore (the same concentration as used in Fig. 2G) or vehicle for 30 min, incubated with Alexa555-conjugated Tf (red) for 10 min at 16°C, transferred back to 37°C and kept for the indicated times. The neurons were acid-washed before fixation to remove surface-bound Tf. (D) Western blot analysis showing Robo1 protein expression in E11.5 dorsal spinal cord neurons treated with vehicle or dynasore, stimulated with 25 pM Slit or control for 10 min. (E) Freshly surface-inserted Robo1 (green) in DCC^{+} (cyan) commissural neurons stained as in Fig. 2E-iii). Maximal-intensity projections of deconvoluted Z-stacks are shown. Surface Robo1 was blocked with anti-Robo1 and unconjugated secondary antibodies, stimulated with Slit or control for 10 min and re-incubated with anti-Robo1 to detect freshly surface-inserted Robo1. Scale bars, 10 μm (top panels) and 5 μm (bottom panels) (A); 20 μm (C); 10 μm (top panels) and 5 μm (bottom panels) (E). All immunofluorescence images were acquired using an Olympus BX61I epifluorescence microscope and deconvoluted.

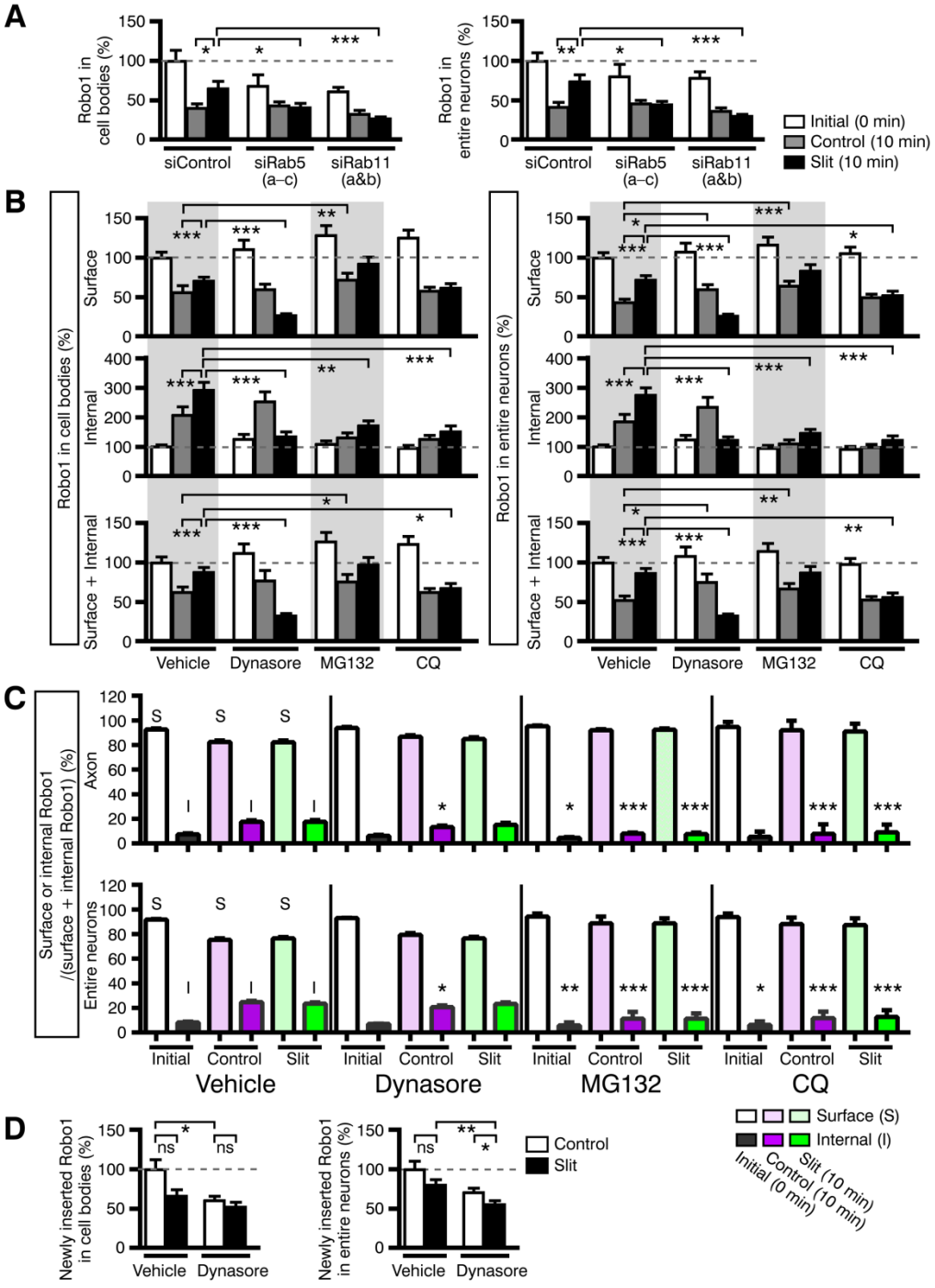

Figure S4. Slit-induced Robo1 endocytic recycling in commissural neurons. (A) Effects of RNAi of Rab5 or Rab11 on Robo1 levels in the cell body and entire neuron [stained as in Fig. 2E-i)]. *n*-values are given in the legend of Fig 2F. **P* < 0.05; ***P* < 0.01; ****P* < 0.001; Mann-Whitney test. (B) Quantification of surface, internal and surface + internal levels of antibody-labelled Robo1 in the cell body and entire neuron [stained as in Fig. 2E-ii) and Fig. S3A]. Robo1 levels in drug-treated neurons were compared to those of vehicle-treated neurons before stimulation (initial). See also Fig. 2G.

(C) Quantification of the two ratios, surface Robo1/(surface + internal Robo1) and internal Robo1/(surface + internal) Robo1, in the distal axon and entire neuron. Endocytosis of antibody-labelled Robo1 that have occurred immediately after the antibody-labelling step (0 min) or 10 min after stimulation were quantified. The initial ratios of internal Robo1/(surface + internal) Robo1 were designated as background levels of internalized Robo1 (see black bars). *$P < 0.05$; **$P < 0.01$; ***$P < 0.001$ (vs. corresponding vehicle-control); Mann-Whitney test. (D) Quantification of Robo1 insertion from the cytoplasm to the surface of the cell body and entire neuron [stained as in Fig. 2E-iii) and Fig. S3E]. Robo1 levels were compared to that of vehicle-treated, control-stimulated neurons. See also Fig. 2H. ns: not significant.

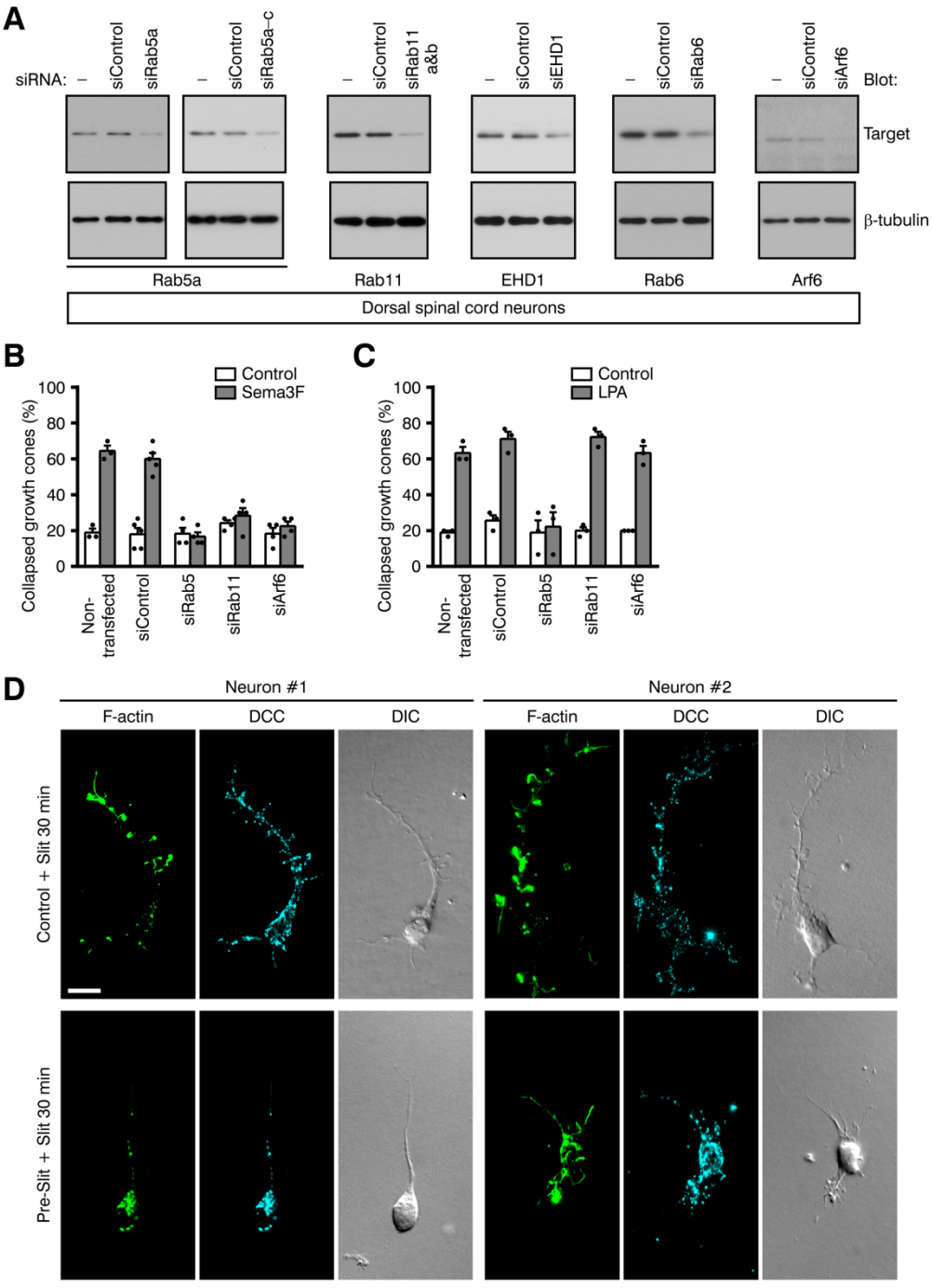

Figure S5. Growth cone collapse responses of commissural neurons to repellents. (A) siRNA-mediated knockdown of endocytic recycling regulators used in this study. Western blot analysis showing that siRNAs targeting Rab5, Rab11, EHD1, Rab6 or Arf6 suppressed expression of the corresponding endogenous protein in primary dorsal spinal cord neurons from E11.5–12.5 embryos following transfection. β-tubulin was used as a loading control. Note that Western blot analyses were performed by using the entire population of cultured neurons including non-transfected neurons and siRNA-transfected ones, whereas the growth cone collapse phenotypes were scored by analysing DCC-

positive neurons successfully transfected with siRNA (shown by red fluorescence of Alexa555-conjugated RNA oligo). (B,C) Growth cone collapse of siRNA-transfected E11.5–12.5 commissural neurons in response to Sema3F (B) or LPA (C) were examined as in Fig. 3A–C (stimulation with 100 μg/ml Sema3F or 1 μM LPA for 30 min). In (B), n = 3, 5, 4, 4 and 4 (experiments) from left to right (30 neurons/experiment). In (C), n = 3 (experiments). (D) Slit-sensitized commissural neurons. Neurons were pre-stimulated with 5 pM Slit or control for 30 min, and further stimulated with 25 pM Slit for 30 min, as in Fig. 3D. Neurons were visualized by staining with Alexa488-conjugated phalloidin (green) and anti-DCC (cyan). Two neurons per group are shown. Slit sensitization drastically affected the morphology of the growth cone, axon and cell body. In Slit-sensitized neurons (bottom panels), growth cone structures were completely lost, and the number of lateral extensions and the axon length were reduced, as compared with unsensitized neurons (top panels). Scale bar, 10 μm. Images in (D) were acquired using an Olympus BX61I epifluorescence microscope and deconvoluted.

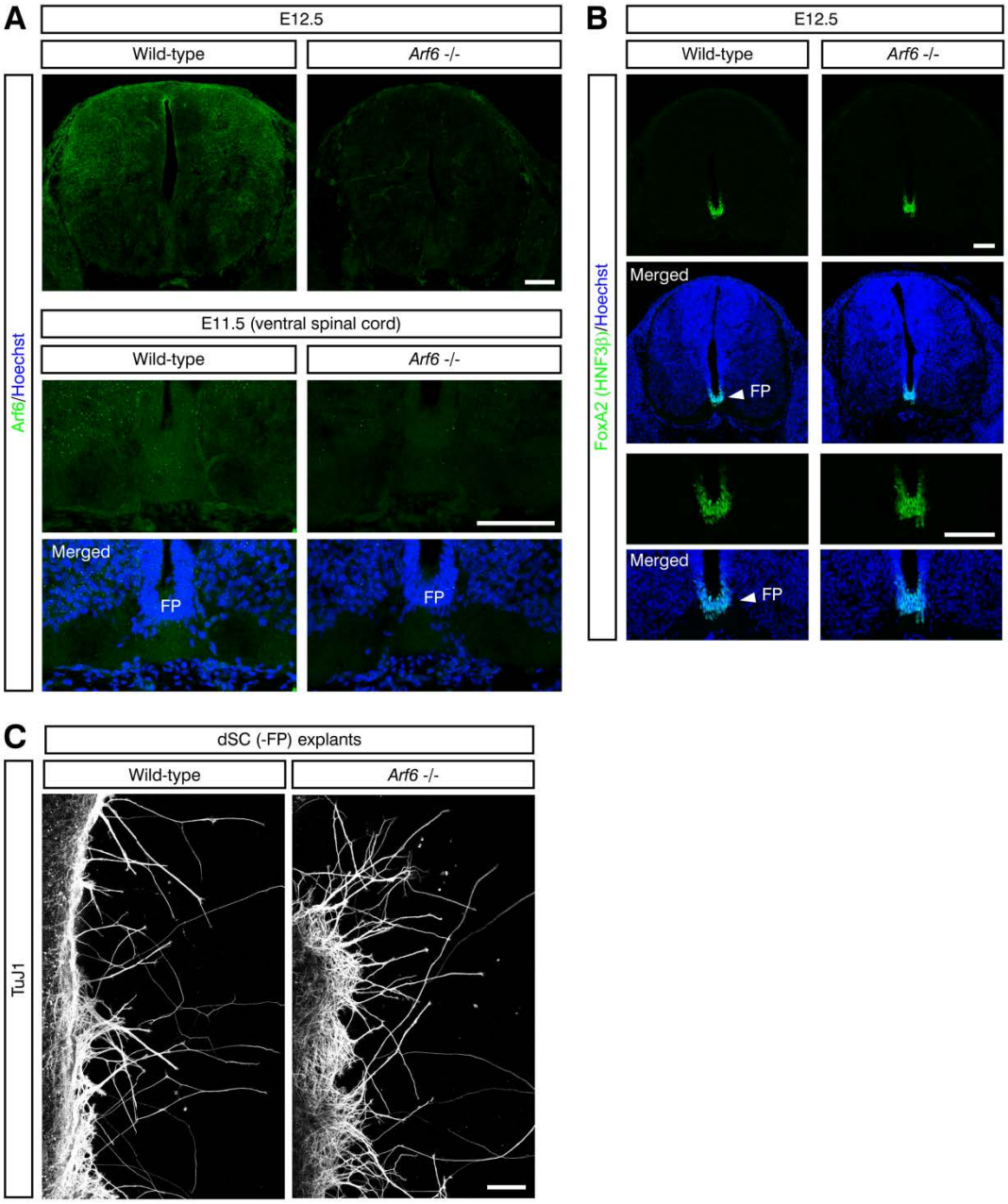

Figure S6. Immunohistochemistry for Arf6 and FoxA2, and spinal cord explants in *Arf6*$^{-/-}$ mutants. (A) Immunohistochemistry for Arf6 of spinal cord sections of E12.5 wild-type and *Arf6*$^{-/-}$ littermates (top panels). Arf6 distribution was detected in the midline-crossing commissural axon region in E11.5 ventral spinal cords (bottom panels). (B) Immunohistochemistry for FoxA2/HNF3β in E12.5 spinal cords. The expression patterns appeared indistinguishable between wild-type and *Arf6*$^{-/-}$ spinal cords. (C) TuJ1 immunostaining of explant cultures of E11.5 dorsal spinal cords. Scale bars, 100 μm (A–C). All images were acquired using a Zeiss LSM780 confocal microscope.

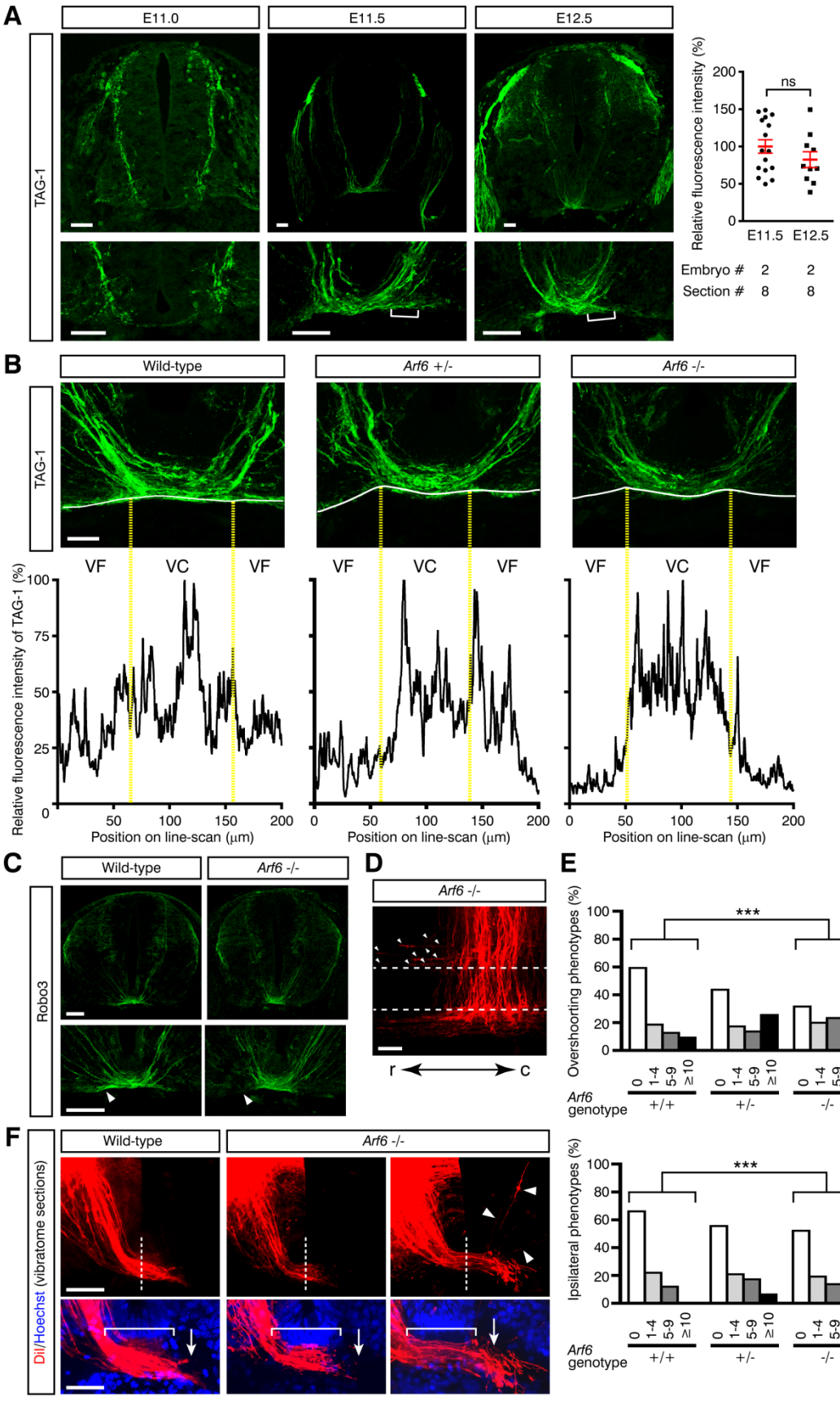

Figure S7. Immunohistochemistry for TAG-1 and Robo3, and DiI labelling in *Arf6*$^{-/-}$ mutants. (A) TAG-1 immunohistochemistry in brachial-level spinal cords at E11.0, E11.5 and E12.5 (left panel). Right panel: quantification of TAG-1 immunofluorescence in the mVF (white brackets in left panels). $P = 0.2249$; Mann-Whitney test. ns: not significant. (B) Relative fluorescence intensity profiles of TAG-1 immunostaining in the spinal cords shown in Fig. 5A. Bottom graphs are line-scans, revealing relative fluorescence intensity of TAG-1 immunosignals through the VF and VC, along the white lines shown in the top panels. (C) Robo3 distribution in E12.5 wild-type and *Arf6*$^{-/-}$ spinal cords at the brachial level. Arrowheads show the mVF region. In wild-type embryos, Robo3 was highly expressed in the pre- and midline-crossing axon segments, but downregulated after midline crossing. In *Arf6*$^{-/-}$ mutants, Robo3 expression in the mVF was lower than that in wild-type embryos. (D) An additional example of anterograde DiI labelling of dorsal commissural axons in E12.5 *Arf6*$^{-/-}$ spinal cords. Axon stalling at the midline and ipsilateral turning were observed (some ipsilateral axons were marked with arrowheads). r: rostral; c: caudal. (E) Quantification of overshooting (top) and ipsilateral (bottom) phenotypes in commissural axons in E12.5 *Arf6*$^{-/-}$ mutants examined by anterograde DiI labelling. Percentages of phenotypes showing indicated numbers of overshooting or ipsilateral axons per DiI injection site are presented as open, shaded and solid black bars. *n*-values are given in the legend of Fig. 5E. ***$P < 0.0001$; χ^2 test. (F) DiI labelling of commissural axons in transverse vibratome sections of E12.5 spinal cords. In the top panels, the midline is shown by dashed lines, and in the bottom panels, the FP is marked with brackets. In wild-type embryos, commissural axons crossed the FP, turning longitudinally on the contralateral side (marked with an arrow; most growth cones disappeared from the image planes after FP crossing). In *Arf6*$^{-/-}$ mutants, many axons were stalled within the FP or at the contralateral FP edge, and the stalled growth cones were visible in these regions on the equivalent image planes; some axons aberrantly entered the contralateral grey matter after FP crossing (arrowheads). Scale bars, 50 μm (A); 25 μm (B); 100 μm (C); 50 μm (D); 100 μm (top panels) and 50 μm (bottom panels) (F). All immunofluorescence images were acquired using a Zeiss LSM780 confocal microscope.

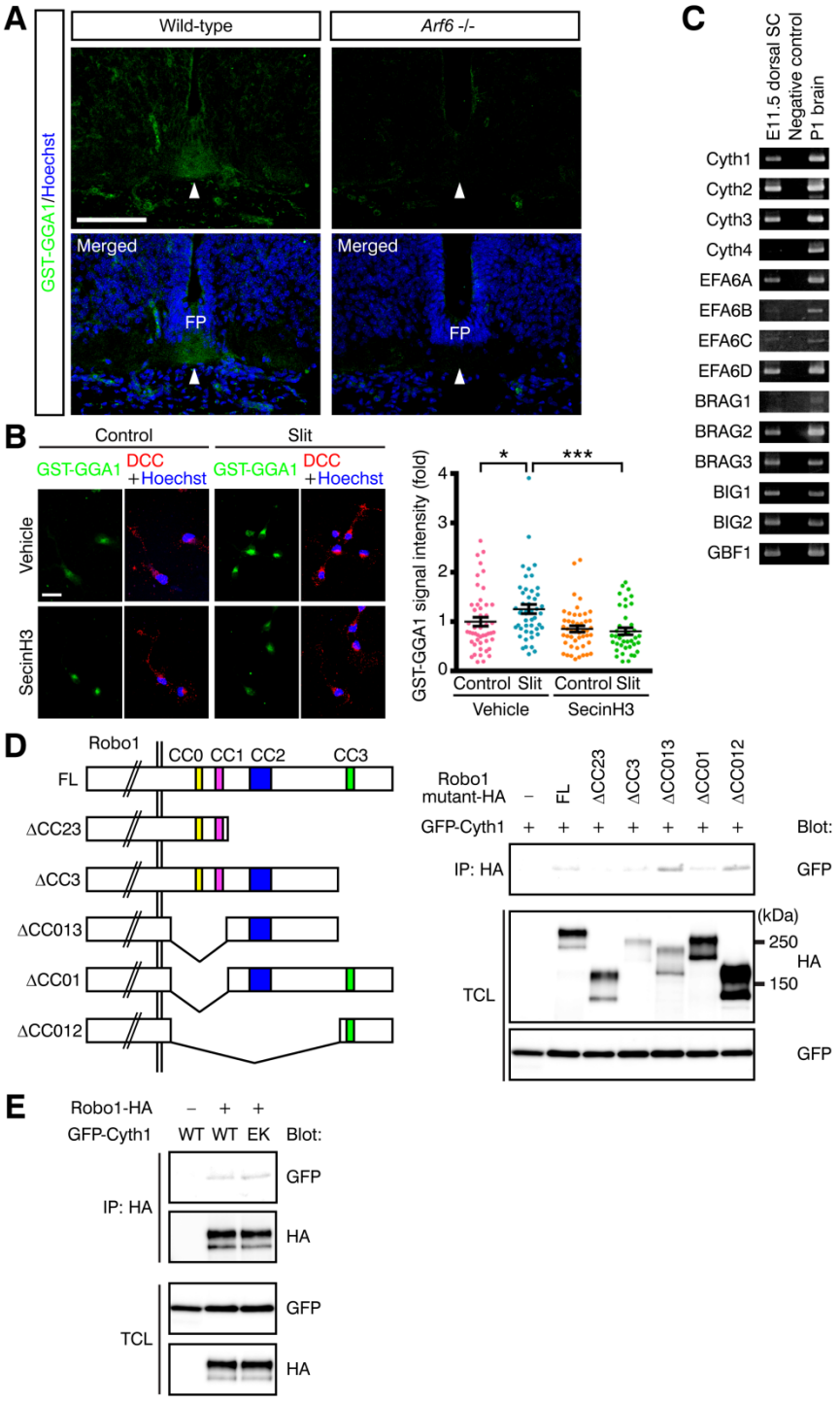

Figure S8. Slit activation of Arf6 in commissural neurons, expression of Arf-GEFs and Robo1-cytohesin interactions. (A) GST-GGA1 immunolabeling of spinal cord sections of E12.5wild-type and *Arf6*$^{-/-}$ littermates. Active Arf GTPases were detected by GST-GGA1. The midline is marked with arrowheads. (B) GST-GGA1 immunolabeling (green) in E12.5 commissural neurons (DCC^{+}; red) stimulated with 25 pM Slit or control for 20 min in the presence or absence of SecinH3. The right graph shows quantification

of GST-GGA1 signal intensity (4 experiments; 10 or more neurons/experiment). *n* = 48, 48, 47 and 40 (neurons) from left to right. **P* = 0.0156; ****P* = 0.0001; Mann-Whitney test. (C) RT-PCR analysis of mRNA expression of Arf-GEFs in E11.5 dorsal spinal cord (SC) neurons. cDNA prepared from postnatal day 1 (P1) whole-brain was used as a positive control. Negative control: PCR without template cDNAs. (D,E) Co-immunoprecipitation was carried out using lysates of HEK 293 cells co-transfected with HA-tagged Robo1 and GFP-tagged Cyth1. Lysates of the transfected cells were immunoprecipitated with anti-HA. The immunoprecipitates and total cell lysates (TCL) were probed with antibodies as indicated by Western blotting. IP: immunoprecipitation. (D) Co-immunoprecipitation of HA-tagged Robo1 deletion mutants with GFP-Cyth1 in HEK293 cells. The left panel shows a schematic illustration of full-length (FL) and deletion mutants of rat Robo1. Residues 1099 to 1657 were deleted in ΔCC23; residues 1455–1657 were deleted in ΔCC3; residues 930–1098 and 1455–1657 were deleted in ΔCC013; residues 930–1098 were deleted in ΔCC01; residues 930–1454 were deleted in ΔCC012. The right panel shows that the CC2 and CC3 motifs of Robo1 mainly contribute to the Robo1-Cyth1 interaction. (E) Co-immunoprecipitation of Robo1-HA with wild-type or catalytically inactive forms of GFP-Cyth1. Scale bars, 100 μm (A); 20 μm (B). All immunofluorescence images were acquired using a Zeiss LSM780 confocal microscope.

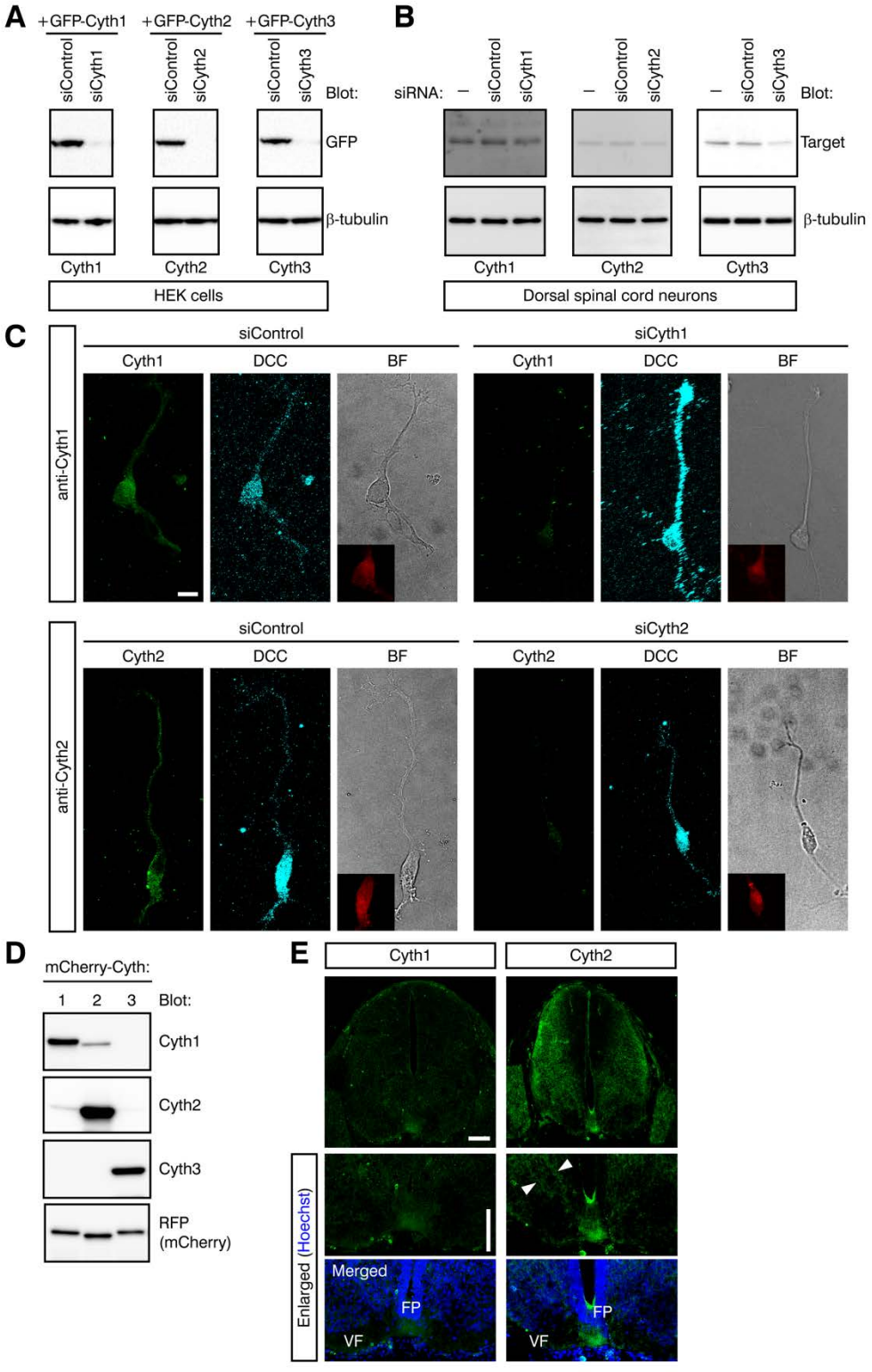

Figure S9. RNAi of cytohesins and immunostaining. (A,B) Western blot analysis showing that siRNA-mediated knockdown of Cyth1–3 suppressed expression of GFP-tagged mouse Cyth1–3 in HEK293 cells (A) and endogenous Cyth1–3 in primary dorsal

spinal cord neurons from E11.5–12.5 embryos (B). (C) Immunocytochemistry with anti-cytohesin antibodies showing that expression of Cyth1 and Cyth2 proteins (green) in E12.5 DCC^{+} (cyan) commissural neurons was suppressed by siRNA transfection. Maximal-intensity projections of confocal Z-stacks together with bright field (BF) images are shown. The efficient introduction of siRNAs into commissural neurons was visualized by fluorescence of Alexa555-conjugated RNA oligo in the soma (red signals in the insets). (D) The specificity of anti-cytohesin antibodies. HEK 293 cells were transfected with plasmids expressing mCherry-tagged cytohesins, and the cell lysates were immunoblotted with the antibodies indicated. (E) Confocal microscopy of expression patterns of Cyth1 and Cyth2 in E12.5 spinal cords. Scale bars, 10 μm (C); 100 μm (E). Images in (C) and (E) were acquired using Leica TCS SP8 and Zeiss LSM780 confocal microscopes, respectively.

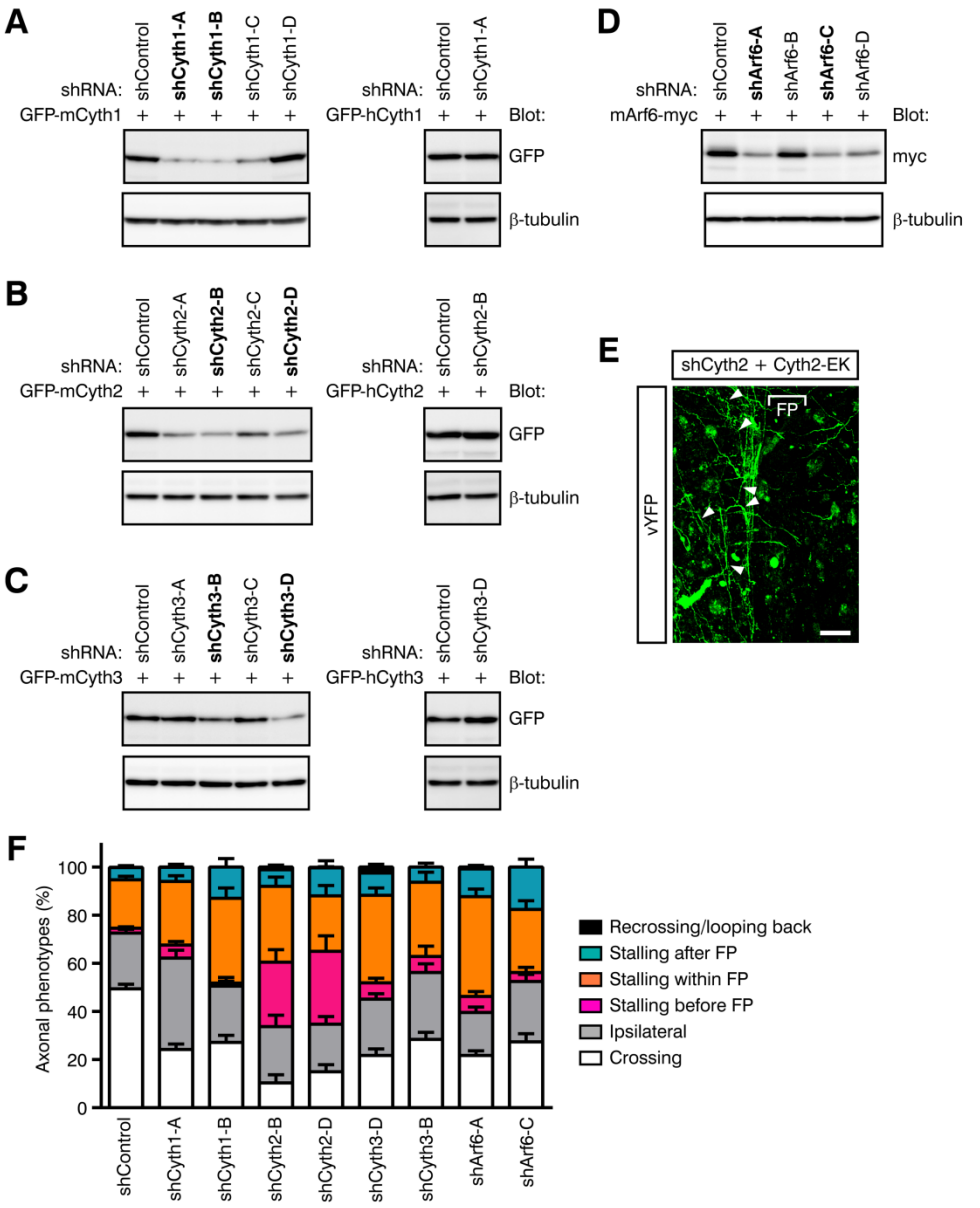

Figure S10. Roles of cytohesin-Arf6 pathways in midline axon pathfinding. (A–D) Western blot analysis showing that shRNAs to Cyth1 (A), Cyth2 (B), Cyth3 (C) or Arf6 (D) suppressed the expression of GFP-tagged mouse cytohesin or myc-tagged Arf6 in HEK293 cells. The shRNAs shown in bold were used in *ex vivo* electroporation. (E) Midline axon trajectories of neurons co-electroporated with shCyth2, *vYFP* and *Cyth2-E156K* plasmids in the spinal cord. Arrowheads show ipsilaterally turning axons. (F) Quantification of effects of two independent sequences of shRNAs against *cytohesins* or *Arf6* on midline axon pathfinding in spinal cord explants. Combined results for the two sequences of shRNAs against each cytohesin or Arf6 are shown in Fig 7C. shCyth1-A, shCyth2-B and shCyth3-D were used for rescue experiments by co-introducing shRNA-resistant human cytohesin expression plasmids. *n* = 91, 30, 14, 23, 23, 21, 12, 33 and 12 (imaging fields) from left to right. Scale bar, 50 μm (E). The image in (E) was acquired using a Zeiss LSM780 confocal microscope.

Table S1

List of PCR primers for detecting expression of mouse Arf-GEFs

Cyth1
(Forward) TTGCTAATGAAATTGAAAGCCTGGGAT
(Reverse) TTCATGGCGATGAATCTCTCCACCGTA

Cyth2
(Forward) AAGTGAAGCTATGAGCGAGGT
(Reverse) TTCATGGCCACAAAGCGCTCCAGG

Cyth3
(Forward) ATTGACAACCTGACTTCAGTG
(Reverse) ATGGTGATGAAGCGCTCAGCGGTG

Cyth4
(Forward) TGTTTGCCCAAATCGACTGCT
(Reverse) TCCTCTACCTTCTGCACGGAG

EFA6A
(Forward) CTGTGGGGACTTCATCGGAAA
(Reverse) TGATCCAGGACTGCATTTGCT

EFA6B
(Forward) CATCAGAGCCCTCAAACTCTGGAC
(Reverse) GAAGCCAAGTGAACATGGTGCTGG

EFA6C
(Forward) ACATGGATGAAGAGAAGCTCCCATGTG
(Reverse) CAGGCCATCCTTAAGGCTGGTGTCAC

EFA6D
(Forward) ATGAGAAGAAGCCGAACGTGT
(Reverse) GCCGCGGATGGATTCTAAGTA

BRAG1
(Forward) ATCTATCGGGATAAGGAGCGA
(Reverse) CGAAGTATGCAGGGTTCTGTG

BRAG2
(Forward) GCTTTCAGCAACGATGTCATC
(Reverse) CACGTGGTCCTCGTTGGTCTT

BRAG3
(Forward) ACGCTCTCCACAGACACCCTG

(Reverse) ACAGCACCGTCTTCATGCCCA

GBF1
(Forward) AGAAGGCACAGCTTTGGTTCC
(Reverse) GCCAGGTCTGGCTGTCTCTTT

BIG1
(Forward) GATGTCTGGCACTGATAATCC
(Reverse) TTATACAGAAGTCGTCTTTGC

BIG2
(Forward) TTCAGGATGACCCAGAGCAGT
(Reverse) ACATTGTACAGCAGCCGCCTC

Table S1. PCR primers used in RT-PCR analysis of Arf-GEFs expression in dorsal spinal cord neurons

Supplemental Materials and Methods

Animals

For timed-pregnancy mating, the day of vaginal plug observation was dated as E0.5, and embryos were staged as described (Yuasa-Kawada et al. 2009a). CD1 (ICR) mice (Charles River and Kyudo) and *Arf6* knockout mice (Suzuki et al. 2006) maintained on the C57BL/6J background were used.

Antibodies, DNA constructs and reagents

Antibodies against Robo1 (rabbit polyclonal, a gift from Drs A. Tamada and F. Murakami), Cyth1 (rabbit polyclonal, a gift from Dr J. Ikenouchi), Cyth2 (rabbit polyclonal, a gift from Dr S. Bourgoin), EHD1 (rabbit polyclonal, a gift from Dr S. Caplan), Arf6 (mouse monoclonal, 3A-1, a gift from Dr S. Bourgoin, and rabbit polyclonal) and lysobisphosphatidic acid (LBPA) (mouse monoclonal, 6C4, a gift from Dr J. Gruenberg) were used for immunostaining and Western blotting. Commercially available mouse monoclonal antibodies used in this study were: anti-DCC (AF5; Calbiochem/Merck Millipore), anti-L1 (2C2; Abcam; ab24345), Alexa647-conjugated anti-β3-tubulin (TuJ1; BD), anti-transferrin receptor (TfR) (H68.4; Thermo Fisher Scientific), anti-HA.11 (Covance), anti-β-tubulin (TUB2.1; Sigma-Aldrich), anti-Rab5 (15/Rab5; BD), anti-Rab11 (47/rab11; BD), anti-syntaxin 6 (30/Syntaxin 6; BD), TAG-1 (4D7; Developmental Studies Hybridoma Bank) and Alexa488-conjugated anti-GST (#617234 ; Merck Millipore). The rat monoclonal antibodies anti-L1 (324; Merck Millipore) and anti-HA (3F10; Roche), the rabbit polyclonal antibodies anti-Robo1 (RP2791; ECM Biosciences and 20219-1-AP; Proteintech), anti-Rab5 (isoform-specific; 11947-1-AP, 27403-1-AP; Proteintech), anti-Rab6 (10187-2-AP; Proteintech) and HRP-conjugated anti-RFP (PM005-7; MBL) and the rabbit monoclonal antibodies anti-FoxA2/HNF3β (D56D6; Cell Signaling Technology) and anti-Cyth3 (EP394Y; Gene Tex) were also used. Alexa-conjugated secondary antibodies and Alexa-conjugated phalloidin and transferrin (Tf) were purchased from Thermo Fisher Scientific. Sema3F protein was purchased from R&D Systems. LPA, dynasore, MDC, MG132 and chloroquine were from Sigma-Aldrich/Merck. SecinH3 was obtained from Merck Millipore.

Green fluorescent protein (GFP)-tagged rat Robo1 was subcloned into pCS2^{+} vector. Wild-type and constitutively inactive, GFP-tagged human Rab5a and Rab11a constructs were gifts from Drs M. Zerial and M. Ehlers. HA-tagged human Arf6, GST-GGA1 and mCherry-tagged human Cyth1–3 plasmids were gifts from Dr K. Nakayama. myc-tagged mouse Arf6 construct was also used to test efficiencies of shArf6. cDNAs encoding mouse Cyth1–3 were obtained from MGC (Mammalian Gene Collection) clones BC057974, BC004662 and BC035296 (transOMIC technologies). GFP-tagged mouse and human wild-type Cyth1–3 were constructed by using PCR with these plasmids as templates. Catalytically inactive, GFP-tagged human Cyth1-E157K, Cyth2-E156K and Cyth3-E161K mutants were generated by site-directed mutagenesis (QuikChange Lightning kit; Agilent Technologies). For rescue experiments in Fig 6C, siCyth2-resistant, GFP-tagged wild-type and mutant Cyth2 constructs were generated by introducing silent mismatches through site-directed mutagenesis. Robo1 deletion mutants

have been previously described (Yuasa-Kawada et al. 2009a; Wong et al., 2001). *Venus-YFP (vYFP)* cDNA was subcloned into pCAG vector to generate pCAG-vYFP.

Cell culture and Slit stimulation

Primary neuronal cultures were prepared from E9.5 or E11.5–12.5 dorsal spinal cords, as previously described (Yuasa-Kawada et al., 2009a). Briefly, neurons were plated on coverslips pre-coated with poly-D-lysine (50 μg/ml, Sigma) and laminin (5 μg/ml, Roche) in Dulbecco's modified Eagle medium (DMEM) supplemented with 10% fetal bovine serum. When purified recombinant Slit2 was used for stimulation of neurons, culture media were replaced with Neurobasal supplemented with B-27 (Thermo Fisher Scientific) on the next day after plating. Neurons were cultured for 2 days in vitro (DIV2; a total of 48 h) before Slit stimulation.

HEK293 cells stably expressing human Slit2-myc or rat Robo1-HA have been described previously (Li et al., 1999). The cell lines have been routinely tested and found negative for mycoplasma contamination. Stimulation of neurons with Slit was as described previously (Yuasa-Kawada et al., 2009a). Slit2 proteins were purified by ion-exchange chromatography using SP-sepharose FF (GE Healthcare) (Guan et al., 2007). Control conditioned media or purified preparations, which were made from parental HEK cells by employing the same procedure as for Slit, were used for the assays in parallel. For Fig. 1A–D and 3, and Fig. S1B–F and S5D, Slit-conditioned media were used; for Fig. 1F,G, 2 and 6, and Fig. S1G,H, S2, S3, S4 and S8B, purified Slit protein was used. In all experiments, Slit was added to the medium to give a final working concentration of 25 pM, except for sensitization assays (Fig. 3E–G and Fig. S5D).

Explant culture

Dorsal parts of spinal cords or intact floor plate (FP)-including half parts (from the cervical to lumbar levels) were dissected out from E11.5 embryos and the pial membrane was removed in Ca^{2+}–Mg^{2+}-free Hanks' solution (HCMF) (see Fig. 1E). With modifications from protocols for retinal explants (Halfter et al. 1983), spinal cords were spread onto black nitrocellulose filters (Sartorius) precoated with 125 μg/ml concanavalin A (Sigma), with the pial side downward and with an extra care taken not to include any FP tissues into the explant (for dorsal spinal cord explants). The filters mounted with spinal cord explants were then reversed, held onto Matrigel (BD; diluted in HCMF to 10% (v/v))-coated coverslips with two metal weights, without embedding in collagen. The explants were cultured with the ventricular side in contact with the surface of the coverslip in a 1:1 mixture of Neurobasal + B-27 and DMEM (Thermo Fisher Scientific) + FBS media for 48 h. Factors to enhance axon growth from spinal cord explants, such as netrins, were not included in our cultures. The cultures were treated with Slit for 10 min and fixed for immunostaining.

siRNAs and shRNAs

Duplex siRNAs to mouse-specific sequences were obtained from Dharmacon, they were as follows: siControl (ON-TARGETplus siCONTROL Non-targeting siRNA #1: D-001810-01), siRobo1#1 (ON-TARGETplus J-046944-10) (Yuasa-Kawada et al., 2009a), pools containing four different sequences of siRNAs against *Rab5* (*5a*: ON-TARGETplus SMARTpool L-040855-00, *5b*: L-040856-01, 5c: L-040857-01, Dharmacon), *Rab6* (ON-

TARGETplus SMARTpool L-040858-01), *Rab11* (*11a*: ON-TARGETplus SMARTpool L-040863-01, *11b*: L-040864-01), *EHD1* (ON-TARGETplus SMARTpool L-040747-01), *Arf6* (ON-TARGETplus SMARTpool L-043217-01), *Cyth1* (ON-TARGETplus SMARTpool L-058480-01) and *Cyth3* (ON-TARGETplus SMARTpool L-062720-01). siCyth2 (Silencer Select, Ambion/Thermo Fisher Scientific) was as previously described (Li et al., 2012). For *ex vivo* electroporation into spinal cords, shRNAs against mouse *Cyth1*, *Cyth2*, *Cyth3* and *Arf6* (in pRS shRNA vector; Origene) were used. Control shRNA (shControl) was also obtained from Origene.

To perform RNAi in dissociated, dorsal spinal cord neurons, a total of 90 pmol of non-labelled siRNAs were mixed with 40 pmol of Block-iT Alexa Fluor Red Fluorescent Control (Thermo Fisher Scientific) and transfected into the neurons (1.0×10^6 cells) resuspended in Opti-MEM (Thermo Fisher Scientific) using 2 μl of Lipofectamine RNAiMAX (Thermo Fisher Scientific) at 37°C for 75 min. Subsequently, the neurons were washed twice before plating, and cultured for 48 h before Slit stimulation. For rescue experiments, siRNA-introduced neurons were re-transfected with plasmids encoding siRNA-resistant, GFP-tagged wild-type or mutant human Rab5a, Rab11a or cytohesins by using Lipofectamine LTX (Thermo Fisher Scientific) on the next day after plating, according to the manufacturer's protocol, and subjected to assays one day later. In the rescue experiments to verify the specificity of siRNA- or shRNA-mediated knockdown of cytohesins, we used constructs encoding the most abundant isoform of cytohesin in the fetal brain: Cyth1 and Cyth2 with GGG motif, and Cyth3 with GG motif (Ogasawara et al. 2000).

Live-cell antibody-feeding assays

Different types of live-cell antibody-feeding assays were performed by using our previously published protocol with minor modifications (Yuasa-Kawada et al., 2009a). For live-cell immunocytochemistry (Fig. 1B, 6D), neurons were stimulated with Slit or control for 10 min, washed once with fresh Neurobasal media supplemented with 20 mM HEPES (Thermo Fisher Scientific), incubated with a rabbit anti-Robo1 antibody (2 μg/ml) (Long et al., 2004; Tamada et al., 2008; Yuasa-Kawada et al., 2009a) for 30 min at room temperature, washed and fixed. Samples were permeabilized and stained with anti-DCC and Alexa-conjugated secondary antibodies.

For Fig. 2D, cultured neurons were incubated with rabbit anti-Robo1 and Alexa555-conjugated Tf (50 μg/ml) for 30 min at room temperature, in order to label Robo1 and the ERC, respectively. After washing, neurons were stimulated with Slit or control for 10 min at 37°C and fixed. The surface Robo1 was blocked with unconjugated anti-rabbit secondary antibody (10 μg/ml; Thermo Fisher Scientific). After permeabilization, internalized Robo1 was detected with Alexa488-conjugated anti-rabbit secondary antibodies. Neurons were also labelled with mouse anti-DCC and Alexa647-conjugated anti-mouse secondary antibodies.

For the live-cell antibody-feeding assay shown in Figs. 2E-i) and 2F, neurons were stained using the same protocol as described previously (Yuasa-Kawada et al., 2009a). Briefly, surface Robo1 was labelled with rabbit anti-Robo1-extracellular domain (2 μg/ml) in fresh culture media supplemented with 20 mM HEPES for 30 min at room temperature. After extensive washing with fresh media, the neurons were immediately fixed (to monitor the initial levels of Robo1 before stimulation), or stimulated with Slit or

control for 10 min and fixed. After permeabilization with 0.2% Triton X-100 in PBS for 2 min, the fixed neurons were immunostained with anti-DCC and Alexa-conjugated secondary antibodies.

For the antibody-feeding assay shown in Fig. 2E-ii) and 2G, neurons were pretreated with dynasore (Macia et al., 2006) (40 μM; 15 min), MG132 (20 μM, 1 h), chloroquine (100 μM; 2 h) or vehicle control, and further treated during the subsequent steps, including antibody-feeding and Slit stimulation, until fixation (see Fig. S2D). Surface Robo1 was labeled with rabbit anti-Robo1 for 30 min at 16°C (to reduce endocytosis). After extensive washing, the neurons were immediately fixed, or stimulated with Slit or control for 10 min at 37°C and fixed. To discriminate between surface Robo1 and internalized Robo1, surface Robo1 (green) was first reacted by incubation of the fixed neurons with Alexa488-conjugated anti-rabbit secondary antibodies without permeabilization for 3 h at room temperature. After three washes with PBS and permeabilization with 0.2% Triton X-100 in PBS for 2 min, the neurons were immunolabeled with mouse anti-DCC for 2 h at room temperature and then with Alexa647-conjugated anti-mouse secondary antibodies and Alexa555-cojugated anti-rabbit secondary antibodies for 2 h at room temperature to visualize DCC (cyan) and internalized Robo1 (red). To calculate surface + internal Robo1 levels, multiple sets of the same types of samples (non-treated neurons before stimulation) were processed in parallel and immunostained for surface Robo1 (green) and internal Robo1 (red) or vice versa. Levels of green and red immunosignals of internal Robo1 were then compared to obtain the ratio of green signals to red signals. Finally, the internal Robo1 levels were obtained on the base of green signals, and the surface + internal levels were calculated.

For the antibody-feeding assay shown in Fig. 2E-iii) and 2H, to visualize newly surface-inserted Robo1, neurons were incubated with rabbit anti-Robo1 (2 μg/ml; it was confirmed that this concentration was saturating for Robo1 immunostaining) for 30 min at 16°C, washed, subjected to incubation with an excess amount of unconjugated anti-rabbit Fab fragment (described as ”Blocking” in Fig. 2E; used at 10 μg/ml; Jackson ImmunoResearch) for 30 min at 16°C to block surface-remaining Robo1 before Slit stimulation and then washed. The neurons were stimulated with Slit or control for 10 min at 37°C, washed and re-incubated with rabbit anti-Robo1 for 30 min at 16°C. After washing, the neurons were fixed, and freshly surface-inserted populations of Robo1 were labelled with Alexa488-conjugated anti-rabbit secondary antibodies. The neurons were permeabilized and incubated with mouse anti-DCC and then with Alexa647-conjugated anti-mouse secondary antibodies. In a negative control experiment, neurons that were live-labelled with rabbit anti-Robo1 and blocked with the unconjugated anti-rabbit Fab were fixed immediately at 0 min (namely without 10-min stimulation). To verify the efficiency to mask initially surface-resident Robo1, such neurons were incubated with Alexa488-conjugated secondary antibodies, without the permeabilization step, and no significant Robo1 signal was detected.

For Fig. S3C, Tf uptake assay was performed as described (Macia et al., 2006).

Growth cone collapse assays and GST-GGA1 immunolabeling

Slit-, Sema3F- or LPA-stimulated growth cone collapse assays were performed as described previously (30 min stimulation except for Slit sensitization assays) (Yuasa-Kawada et al., 2009a). Sema3F protein or LPA was used at 100 μg/ml or 1 μM,

respectively. Growth cones were defined by the presence of lamellipodia and/or filopodia. Neurons were selected randomly based on fluorescence of anti-DCC and/or Block-iT Alexa Fluor Red Fluorescent Control. For drug-treatment experiments, neurons were pre-incubated with dynasore (40 μM; 15-min pretreatment), MDC (10 nM; 30-min pretreatment), SecinH3 (10 μM; 30-min pretreatment) or vehicle control (the maximal concentrations for each drug that did not affect growth cone morphology in commissural neurons in the absence of Slit were determined). Subsequent growth cone collapse assays were performed in the presence of the drug. In each experimental group, at least three independent experiments were performed (30 neurons per group were scored in each experiment).

For GST-GGA1 immunolabeling, neurons were stimulated as indicated, fixed, treated with 50 mM NH_4Cl and permeabilized with 0.2% Triton X-100 in PBS. Neurons were then immunolabeled as described with some modifications (Harrington et al., 2011). Briefly, neurons were incubated with 8 μg/ml purified GST-GGA1 probe overnight at 4°C. The neurons were washed and incubated with anti-DCC for 2 h at room temperature, and with Alexa555-conjugated anti-mouse secondary antibodies for 2 h at room temperature, followed by incubation with Alexa488-conjugated anti-GST antibody for 2 h at room temperature. Z-stack images were taken with an LSM780 microscope, summed and quantified.

Immunohistochemistry

Embryos were fixed overnight at 4°C in 4% PFA/PBS, washed with PBS, incubated in 5% and 30% sucrose/PBS overnight and embedded in a mixture of OCT and 30% sucrose/PBS (the volume ratio of 3:1). Spinal cord transverse cryosections at brachial to abdominal levels (20 μm) were collected on Superfrost glass slides (Matsunami) and air-dried overnight. The slides were used directly for immunostaining or kept at -80°C until use. Slides were blocked in PHT (0.1% Triton X-100 in PBS containing 1% heat-inactivated goat serum) for 1 h at room temperature, incubated with the primary antibody in PHT overnight at 4°C, washed 3 times with PBS, incubated with the secondary antibody in PHT for 2 h at room temperature, washed 3 times with PBS and coverslip-mounted with Permafluor (Thermo Fisher Scientific). For immunostaining for Cyth1 and Cyth2, cryosections were unmasked by microwave irradiation in 10 mM citric acid (pH6.0). All controls were wild-type littermates of the mutant embryos.

Images were taken with an LSM780 microscope, and quantitative analyses were performed by an individual blind to the genotype, using MetaMorph software. For quantification of immunoreactivity of TAG-1 and Robo1 in the medial ventral funiculus (mVF), the signal intensity in a rectangular region (100 x 15 μm) was measured on both sides of a brachial-level spinal cord section per embryo after background subtraction and threshold setting, and then normalized to the mean intensity obtained from each of the age-matched wild-type littermate embryos.

For GST-GGA1 immunolabeling, cryosections were blocked as described above, and incubated with 8 μg/ml purified GST-GGA1 probe overnight at 4°C and with Alexa488-conjugated anti-GST antibody for 2 h at room temperature.

DiI labelling

Spinal cords of E12.5–14.5 wild-type and *Arf6*$^{-/-}$ embryos were fixed in an open-book configuration with 4% PFA/PBS overnight. Alternatively, transverse vibratome sections (100 μm-thick) of E12.5 embryos were prepared (wild-type: $n = 4$; *Arf6*$^{-/-}$: $n = 3$). For anterograde axon labelling, the dorsal spinal cords were injected with small crystals of DiI (Thermo Fisher Scientific) and the DiI was allowed to diffuse for two days to label commissural axons anterogradely along their entire length. For retrograde axon labelling, the VF regions of spinal cords were injected with DiI crystals and the DiI was allowed to diffuse for three days to label ipsilateral axons and contralateral commissural axons, as well as their cell bodies. Samples were observed with an LSM710 or LSM780 microscope.

Cell-surface biotinylation, Arf6 pulldown assays, co-immunoprecipitation and Western blotting

Cell-surface biotinylation, Arf6 pulldown assays, co-immunoprecipitation and Western blotting were performed essentially as described in previous studies (Hanai et al., 2016; Santy and Casanova, 2001; Yuasa-Kawada et al., 2009a, 2009b).

Briefly, cell-surface biotinylation in primary dorsal spinal cord neurons from E12.5 embryos was performed by using the Cell Surface Protein Isolation kit (Pierce/ThermoFisher Scientific). After a brief wash with ice-cold PBS following stimulation, cells were incubated in 250 μg/ml EZ-Link-Sulfo-NHS-SS-Biotin for 30 min at 4°C. Addition of a quenching solution containing glycine terminated the biotinylation reaction. Cells were then washed with cold Tris-buffered saline and lysed in a buffer (50 mM Tris-HCl, pH7.4, 150 mM NaCl, 1% Triton X-100) containing a protease inhibitor cocktail (Roche). Lysates were then incubated with Neutravidin-agarose at 4°C overnight, and biotinylated proteins were subsequently eluted from the beads by heating at 95°C for 5 min in 2x Laemmli buffer with 50 mM DTT.

To monitor Arf6 activation in response to Slit in control or Robo1-HA–expressing HEK293 cells, human wild-type Arf6-HA–expressing plasmid was transfected. After serum starvation for 16 h, cells were stimulated with Slit for the indicated times and lysed. Active, GTP-bound Arf6 was captured with GST-GGA1 (Hanai et al., 2016; Santy and Casanova, 2001) and detected by immunoblotting with anti-Arf6. For Arf6 pulldown in primary cultures of mouse cortical neurons, the endogenous active Arf6 was detected with anti-Arf6. For co-immunoprecipitation between Robo1 and cytohesins in the cell extracts prepared from embryonic mouse whole-brain, including the hindbrain and rostral spinal cord (from the cervical to brachial levels), Robo1 protein was immunoprecipitated with a rabbit polyclonal antibody against the C-terminal domain of Robo1 (ECM Biosciences) in a buffer containing 1% NP-40 and 1% sodium deoxycholate and detected by immunoblotting with another anti-Robo1 rabbit polyclonal antibody (Proteintech). Pulldown samples, immunoprecipitates and cell lysates were resolved on an SDS-PAGE gel, immunoblotted and detected with ECL Plus, ECL Prime, ECL Select, ECL Advance kit (GE Healthcare) or Western Lightening ECL Pro (Perkin Elmer) using the X-ray films, LAS3000 or LAS4000mini (GE Healthcare). Can Get Signal kit (Toyobo) was used for detecting weak immunosignals.

RT-PCR

Total RNA was extracted from cultured dorsal spinal cord neurons from E11.5 embryos by using Illustra RNAspin mini RNA isolation kit (GE Healthcare) and reverse-transcribed with Superscript reverse transcriptase II (Thermo Fisher Scientific) and random primer at 42°C for 60 min. cDNAs were subjected to 33 cycles of PCR, each cycle consisting of 95°C for 2 min, 95°C for 30 sec, 56°C (Cyth1, Cyth3, BRAG1–3, EFA6A and EFA6C) or 60°C (Cyth2, Cyth4, EFA6B, EFA6D, GBF1, BIG1 and BIG2) for 30 sec and 74°C for 60 sec, followed by 74°C for 10 min, using Ex Taq polymerase. The primers used are listed in Table S1.

***Ex vivo* electroporation and spinal cord explant culture**

Spinal cords of E11.5 embryos were injected with a solution containing shRNA constructs (2 μg/μl) and pCAG-vYFP (0.4 μg/μl). For rescue experiments, GFP-tagged, human wild-type or catalytically inactive mutant cytohesin expression plasmid (1 μg/μl) was co-introduced into the embryos. Immediately thereafter, embryos were electroporated with three 50-ms pulses of 20 V at 50-ms intervals using NEPA21 (NEPA GENE) and forceps-type electrodes (CUY665P9-6-2-5). The spinal cords were dissected out, and their 'closed-book' preparations were covered with collagen matrix (Koken) and cultured in media consisting of 45% Opti-MEM I, 50% F-12, 40 mM glucose and 5% horse serum (Sabatier et al., 2004) (see Fig. 7A). After culturing for 4 days (with media change daily) and dissecting out from the collagen gel, the spinal cords were fixed in an open-book configuration with 4% PFA/PBS. Confocal Z-stacks of green-channel images for visualizing vYFP signals and differential interference contrast (DIC) images were taken with the LSM780 microscope to define the accurate position of the FP. For quantification, the number of axons that exhibited turning contralaterally (crossing) or ipsilaterally, stalling or re-crossing/looping back in each imaging field were counted and presented as the percentage compared to the total number of vYFP-positive axons. Overshooting phenotypes were excluded from analysis, because we detected these phenotypes in the tissue areas damaged by electroporation and/or manipulation, even in shControl-targeted embryos.

The number of axons traced and scored was 3024 (from 34 embryos) for shControl-electroporated explants, 1475 (11 embryos) for shCyth1, 1032 (11 embryos) for shCyth2, 867 (7 embryos) for shCyth3, 456 (5 embryos) for shCyth1 + Cyth1-WT, 467 (6 embryos) for shCyth1 + Cyth1-E157K, 245 (4 embryos) for shCyth2 + Cyth2-WT, 377 (4 embryos) for shCyth2 + Cyth2-E156K, 411 (6 embryos) for shCyth3 + Cyth3-WT, 448 (5 embryos) for shCyth3 + Cyth3-E161K and 1543 (11 embryos) for shArf6.

Supplemental References

Guan, C. B., Xu, H. T., Jin, M., Yuan, X. B. and Poo, M. M. (2007). Long-range Ca^{2+} signaling from growth cone to soma mediates reversal of neuronal migration induced by Slit-2. *Cell* **129**, 385–395.

Halfter, W., Newgreen, D. F., Sauter, J. and Schwarz, U. (1983). Oriented axon outgrowth from avian embryonic retinae in culture. *Dev Biol.* **95**, 56–64

Harrington, A. W., St Hillaire, C., Zweifel, L. S., Glebova, N. O., Philippidou, P., Halegoua, S. and Ginty D. D. (2011). Recruitment of actin modifiers to TrkA endosomes governs retrograde NGF signaling and survival. *Cell* **146**, 421–434.

Li, J., Malaby, A. W., Famulok, M., Sabe, H., Lambright, D. G. and Hsu, V. W. (2012). Grp1 plays a key role in linking insulin signaling to Glut4 recycling. *Dev. Cell* **22**, 1286–1298.

Santy, L. C. and Casanova, J. E. (2001). Activation of ARF6 by ARNO stimulates epithelial cell migration through downstream activation of both Rac1 and phospholipase D. *J. Cell. Biol.* **154**, 599–610.